ON THE MOTION OF AIR THROUGH THE STRATOSPHERIC POLAR VORTEX

G. L. Manney, R. W. Zurek,

Jet Propulsion Laboratory/California Institute of Technology,

A. O'Neill,

Centre for Global Atmospheric Modelling, Reading UK,

R. Swinbank,

Meteorological Office, Bracknell UK

Submitted to

Journal of the Atmospheric Sciences,

UARS Special Issue

Abstract

Trajectory calculations using horizontal winds from the United Kingdom Meteorological Office data assimilation system, and vertical velocities from a radiation calculation are used to simulate the three-dimensional motion of air through the stratospheric polar vortex, for several northern hemisphere (NH) and southern hemisphere (SH) winters since the launch of UARS. Throughout the winter, air from the upper stratosphere moves poleward and descends into the middle stratosphere. In the SH lower to middle stratosphere, strongest descent occurs near the edge of the polar vortex. The NH shows a similar pattern in late winter, but in early winter strongest descent is near the center of the vortex. Strong barriers to latitudinal mixing exist above ≈420 K throughout the winter. Below this, the polar night jet is weak in early winter, so air that descends below that level mixes between polar and middle latitudes. In late winter, parcels descend less, and the polar night jet moves downward, so there is less latitudinal mixing. The degree of mixing in the lower stratosphere thus depends strongly on the position and evolution of the polar night jet,

The computed trajectories provide a three-dimensional picture of air motion during the final warming, Large fragments of vortex air are drawn out into increasingly narrow tongues in low latitudes. In the lower stratosphere; strong PV gradients remain, and the majority of air parcels remain confined, into December in the SH and April in the NH, well after the vortex breaks up in the mid-stratosphere.

1. Introduction

Several recent studies address aspects of air motion through the stratospheric polar vortex, and mixing between vortex and extra-vortex air. Bowman (1993a) showed that in a barotropic model there is little transport out of the Antarctic polar vortex by planetary scale waves prior to vortex breakdown. Chen and Holton (1994), and Bowman and Chen (1994) address aspects of mixing by barotropically unstable waves that are characteristic of the middle and upper stratosphere in winter, and show that, again, there is little transport across the vortex edge due to these waves. Several recent studies (Bowman 1993b, Chen et al. 1994, Chen 1994) use horizontal winds derived from data to explore isentropic mixing across the vortex edge in the Southern Hemisphere (SH) lower stratosphere. These studies suggest there is a transition in the lower stratosphere in late winter around the 400 K isentropic surface, above which the vortex is nearly completely isolated from mid-latitudes, and below which more mixing occurs. Dahlberg and Bowman (1994) show similar analyses for the Northern Hemisphere (NH) lower stratospheric vortex; despite greater variability of the Arctic polar vortex, their results are similar to those for the Antarctic vortex, showing little transport across the vortex boundary above ≈425 K during winter, Waugh et al. (1994) and Plumb et al. (1994) use high resolution isentropic simulations to explore specific events in the Arctic winter when air was ejected from the polar vortex in the lower stratosphere, and when mid-latitude air intruded into the vortex. Pierce and Fairlie (1993) examined chaotic mixing near the vortex edge using three-dimensional (3-d) winds from a General Circulation Model simulation of the Arctic winter, and conclude that mixing of air near the vortex edge could have a significant impact on the distribution of trace constituents in the lower stratosphere.

Fisher et al. (1993) explore more general aspects of air motion, using winds from a 3-d model of the stratosphere and mesosphere to examine the motion of a large number of air parcels throughout the Antarctic winter. They obtain a picture of poleward and

downward motion of parcels throughout the winter, with little mixing of parcels initialized on different isentropes. Parcels initialized in the mesosphere (≈0. 1 hPa) descend as far as= 100 hPa in the polar regions over a period of 5 months, beginning in early winter.

Both the degree of horizontal mixing and the amount and patterns of descent in the winter lower stratosphere remain subjects of considerable debate, as discussed by Randel (1993). From the limited data available, arguments have been made for both greater (e.g., Hartmann et al. 1989, McIntyre 1989, Schoeberl et al. 1989, 1992) and lesser (e.g., Tuck 1989, Tuck-et al. 1992, Proffitt et al. 1989, 1992) degrees of isolation of the lower stratospheric vortex, and correspondingly smaller or larger descent rates. Various locations of strongest descent in the lower stratosphere with respect to the edge of the polar vortex have also been suggested (e.g., Schoeberl et al. 1992, Tuck et al. 1993, Russell et al 1993).

We use horizontal winds derived from observations using a data assimilation system, and vertical velocities derived from a middle atmosphere radiation code, to examine the 3-d motion of air in the winter stratosphere, focusing on the polar regions and their interaction with mid-latitudes. The meteorological data are from the United Kingdom Meteorological Office's data assimilation system (Swinbank and O'Neill 1994), available since shortly after the launch of UARS. We compare results for NH and SH winters, and for early and late winter, and examine the relationship of isolation of the lower stratospheric vortex to the structure and evolution of the polar night jet. We also describe the 3-d motion of air parcels during the final warming in both hemispheres. These simulations give an overall view of the 3-d patterns of air motion for several periods of interest observed by UARS.

2. Data and Analysis

The trajectory calculations are done in isentropic coordinates using horizontal winds and temperatures from the United Kingdom Meteorological Office (UKMO) data assimilation system (Swinbank and O'Neil] 1994) that are available through the Upper Atmosphere Research Satellite (UARS) project. The meteorological data assimilated by the UKMO for the stratosphere do not include UARS data at present, but are based on available conventional meteorological data. One advantage of data assimilation products is that they provide consistent global horizontal wind components.

Cross-isentropic flow is computed using a recent version of the middle atmosphere radiation code MIDRAD, an earlier version of which is described by Shine (1987). This code provides a reasonable balance between precision and the computational efficiency required when computing trajectories for extended simulations. Temperatures in the radiation code are from the UKMO data. The radiation code's climatological ozone is used, since UARS ozone observations do not provide complete coverage of the periods of these simulations. A comparison of heating rates calculated using this climatology with those calculated using MLS ozone for Aug 1992 (Feb 1993) in the SH (NH) shows differences in zonal means at levels below $\approx$3 hPa of less than $\approx$0.1 K/day poleward of $\approx 30^{0}$ latitude. At these times the net heating rates are dominated principally by radiative cooling due to $C0_2$ and so are most sensitive to temperature. The horizontal and vertical motions are not constrained to be conservative, but a check of the fields indicates that they are nearly so and are within the uncertainties implicit in the use of the trajectories to represent mass motion,

The trajectory code is described briefly by Manney et al. (1994a); it is adapted from that used by Fisher et al. (1993), and uses a standard fourth-order Runge-Kutta scheme. Winds and temperatures are interpolated linearly in time from the once daily values to the trajectory time step (1/2 hour). Heating rates are recalculated every 3 hours using

interpolated temperatures, and are interpolated linearly to the trajectory time step between calculations. As noted by Bowman (1993b) and Morris et al. (1994), it is expected that errors in trajectories will be dominated by errors in the wind field, rather than by numerical truncation error. The domain of the trajectory model is from 375 K through 1900 K, and from the pole in the hemisphere of interest to 28^{o} latitude in the opposite hemisphere. Parcels that move outside these boundaries cease to be advected; no new parcels are introduced into the domain during a simulation.

The Rossby-Ertel potential vorticity (PV) is used to describe the polar vortex and to compare with the positions of air parcels. PV is calculated from UKMO winds and temperatures as described by Manney and Zurek (1993). To facilitate examination of a deep vertical range, for some plots PV is scaled in "vorticity units" (Dunkerton and Delisi 1986, Manney and Zurek 1993) by dividing by a standard atmosphere value of the static stability; this gives a similar range of values for PV on isentropic surfaces throughout the stratosphere.

Approximately 40,000 air parcels are initialized cm a latitude/longitude grid covering one hemisphere on 12 isentropic surfaces throughout the stratosphere: 420,465, 520, 585,655,740, 840,960, 1100, 1300, 1450, and 1700 K. The periods examined are shown in Table 1. During early winter the polar vortex is developing and expanding, and minor warming events are common in both hemispheres (Manney et al. 1994, paper in preparation). Stronger warming events occur in late winter and spring, including the final warming in spring. During all of the winter periods, air parcels originating in the middle and upper stratosphere descend relatively rapidly, so the upper stratosphere becomes deviod of parcels in the longer simulations. Therefore, in order to more closely examine the SH final warming, additional trajectory calculations were initialized in mid-spring.

It is convenient in describing the motion of parcels with respect to the polar vortex to bin the parcels according to their PV at the start of the run. This is done using the scaled PV mentioned above. Although over the entire depth of the stratosphere, the

values of scaled PV outlining the vortex edge change slightly, on a given day, the same value is a reasonable approximation to the vortex edge over the vertical range experienced by parcels started on any one level in a simulation of one to two months. Diabatic and other non-conservative processes of course alter the PV location of the vortex edge significantly on this time scale, as will be discussed further below. To examine mixing characteristics of the stratospheric flow, we have calculated both PV dispersion (Dahlberg and Bowman 1994) and latitude dispersion (Schoeberl et al. 1992, Bowman 1993a,b) of the air parcels. Latitude dispersion is calculated from ensembles of parcels binned by PV, similar to Schoeberl et al. (1992), While binning by latitude is informative in the SH cases described by Bowman (1993a,b), where the polar vortex is relatively symmetric, the NH polar vortex is typically sufficiently distorted that binning by latitude serves to obscure characteristics of the flow, so binning by PV is preferred.

3. **General Features of Air Motion**

Figure 1 shows O/latitude cross-sections of parcel positions after running the trajectory code for 66 (55) days for early (late) winter. All parcels poleward of $\approx 30^{O}$ experience descent, Consistent with Fisher et al.'s (1993) model results for the SH winter, the SH results in both early and late winter show rapid descent and poleward motion of parcels that start in the upper stratosphere, with relatively little mixing of the parcels started at different levels, The NH cases show similar descent and poleward motion, but due to greater variability in the NH, there is much more mixing of the parcels in the middle and upper stratosphere in early winter, and throughout the stratosphere in late winter. The overall amount of diabatic descent in early winter appears similar for all 4 cases shown here, with parcels in the NH descending slightly farther than in the SH, and parcels in the SH during 1992 descending slightly farther than in 1993. In the late winter SH, parcels descend considerably more in 1992 than in **1993.** Throughout the 1993 SH

winter, there was less planetary scale wave activity than in the 1992 SH winter; this is apparent in Fig. 1, especially in the upper stratosphere, in that there is much less spreading of the parcels in mid-latitudes, and in late winter, less spreading of parcels into the polar regions in 1993.

In the SH it is evident that at levels below ≈850 K, the strongest diabatic descent is at ≈50--60° latitude, near the edge of the polar vortex. Above this, strongest descent is near the pole. It will be seen that this is sometimes the case in the NH. Only one example is shown of the NH late winter circulation; a very large degree of interannual variability is expected in the late winter NH. The example shown here is a relatively active year with strong stratospheric warmings during February and March (Manney et al. 1994b). Manney et al. (1994c) show evidence from passive tracer measurements that there is considerably less descent in Feb/Mar 1992, a much less active time period, than Feb/Mar 1993.

Figure 2 shows, for one early winter and one last winter period in each hemisphere, plots similar to Figure 1, but as a function of pressure rather than θ. From the initial and final altitudes of the parcels we obtain rough estimates of the average geometrical vertical velocities during these time periods, summarized in Table 2, As was the case when viewed in isentropic coordinates, the largest geometrical vertical velocities are usually ≈50° to 60° latitude, near the edge of the polar vortex. In the top few levels shown here, largest descent is seen near the pole. In both early and late winter, slightly larger vertical velocities are estimated in the SH than in the NH. The estimates for the late winter time period are consistent with estimates by Santee et al. (1994, paper in preparation) from UARS passive tracer data, The values estimated for the Arctic are also similar to those deduced by Schoeberl et al. (1992) for the 1989 Arctic mid-winter; values given by Schoeberl et al. for the Antarctic late winter of 1987 are= 1/2-2/3 the values estimated here. Overall, the estimated vertical velocities are somewhat less than the residual vertical velocities estimated by Eluszkiewicz et al. (1994, this issue) using MLS ozone,

temperature and water vapor data in a more detailed radiative transfer model.

Figure 3 shows plots like those in Fig. 1 for continuations of the runs started in August in the SH, and for runs started near the beginning of November in the midst of the SH final warming. By the beginning of December, near the end of the SH final warming, parcels started at 1700 K in mid-August have descended as far as ≈650 K, The plots of parcels started in November show that during the final warming, parcels in the mid-stratosphere are still descending in the polar regions (between ≈600 and 1300 K, poleward of ≈60^{O}S).

Figures 4 through 6 show in more detail the patterns of descent experienced by the parcels. Figure 4 shows the potential temperature of parcels started at 465, 840, and 1100 K, 55 days after the beginning of the runs started in early winter, and Figure 5 shows the corresponding plots for runs started in late winter. At 465 K, the parcels in the SH descend furthest near or outside the edge of the polar vortex. The same pattern can be detected in the NH, although the descent in the center of the vortex is stronger, and the difference in descent rates between the center and the edge of the vortex is smaller. Over the 55 days shown, the largest decreases in potential temperature in the NH are =10-15 K greater than in the SH in the lower stratosphere.

At 840 K, there is strong descent in the center of the vortex, and along or outside the vortex edge, usually separated by a region of weaker descent. In the SH early winter, strongest descent is in the center of the vortex, with another region of strong descent outside the edge of the vortex. In the SH late winter the strongest descent is inside the edge of the vortex. In the NH, strongest descent is in the center of the vortex when wave activity is weaker (i.e., early winter 1992/93) and along the edge of the vortex when wave activity is strong (i.e., early winter 1993/1994 and late winter 1993). During stratospheric warmings (periods of strong wave activity), the strongest descent is observed to be between the cyclone and anticyclone (Manney et al. 1994a,b), consistent with this pattern. At 1100 K, strongest descent is in the center of the vortex, except in the NH during

periods of particularly strong wave activity (i.e., Feb/Mar 1993).

Figure 6 shows the potential temperatures of parcels started at 465, 840 and 1100 K in August in the SH, near the end of the final warming, Over approximately 4 months from August through November, the parcels that descend most from the 465 K level are those along and outside the edge of the vortex. Those that descend most from 840 K and 1100 K levels are those in the center of the vortex,

Figure 7 summarizes some of these characteristics of descent, showing time series of the average change in potential temperature of parcels as a function of initial PV started at 840 and 465 K, The region of strongest PV gradients is generally between 1.() and 1.4 x 10-4 s^{-1} in these units; it will be seen later that this is an appropriate definition of the vortex edge based on mixing characteristics. Table 3 summarizes the average changes in potential temperature from these and similar plots (not shown) for other levels. In the early winter lower stratosphere, there is diabatic descent of ≈0.6 to 0.8 K/d in potential temperature ($d\theta/dt$), with slightly stronger values in the NH than in the SH, and with strongest descent in the center of the vortex in the NH and at the edge in the SH. In late winter lower stratosphere, diabatic descent is ≈0.4 to 0,5 K/d in the NH and ≈0.3 to 0.4 K/d in the SH; in both hemispheres strongest descent is near the edge of the vortex. In spring (Nov/Dee) in the SH, diabatic descent in the lower stratosphere is ≈0.2 to 0.3 K/d, Strahan et al. (1994) diagnosed values of ≈0.5 to 0.7 K/d in mid-winter in the NH from aircraft measurements in the 1992 winter, roughly consistent with these values. Average descent rates at 840 K in the mid-stratosphere range from ≈2 to 4 K/d, and at 1300 K, in the upper stratosphere, from ≈8 to 10 K/d. In the upper stratosphere, strongest descent is always at the center of the vortex; in the mid-stratosphere, strongest descent is at the edge of the vortex in the late winter SH; in the NH late winter, there are regions of strong descent at the center and the edge of the vortex. In the middle and lower stratosphere diabatic descent is stronger in the NH than in the SH, a consequence of higher NH temperatures and stronger NH wave activity. However, because of the differences in

temperature structure and evolution in the two hemispheres, this does not imply that geometrical vertical velocities are larger in the NH (see Table 2).

4. Mixing properties and vortex containment

To examine the mixing of the air parcels, we show the latitude dispersion of parcels in PV bins as described above. Figure 8 shows time series of dispersion for parcels started at 465 and 840 K, for early winter, late winter, and SH spring periods, Only one year is shown for each season and hemisphere; overall features are similar in the year that is not shown. A minimum in the dispersion indicates the edge of the polar vortex, where there is a barrier to mixing (e.g., Schoeberl et al. 1992, Bowman, 1993b). At the beginning of each time series, as PV increases there is an abrupt decrease in dispersion at a (scaled) PV of $=1.0 \times 10^{-4}$ S-l at 465 K, and $=1.4 \times 10^{-4}$ s-^{1} at 840 K, showing the location of the polar vortex. Increases in the dispersion for PV values higher than this are coincident with stratospheric warmings; Fishbein et al. (1993) and Manney et al. (1993) show minor warmings in the SH in Aug/Sep 1992; Manney et al. (1994b) show warming events in Feb/Mar 1993. In early winter in the NH there are strong minor warmings in both Dec 1992 and Dec 1993 (Manney et al. 1994, paper in preparation), with a major warming in late Dec 1993/early Jan 1994. In the NH, strong warmings result in a shift in the edge of the vortex (as defined by the limited dispersion) to higher PV values, $\approx 1.8 \times 10\text{-}4$ s^{-1} at 840 K in early Mar 1993 and late Dec 1993 (not shown); at 465 K, a similar shift can be seen in Mar 1993. During stratospheric warmings, the region of strongest PV gradients shifts to higher latitudes (i.e., the vortex shrinks in size) and to higher PV values (i.e., the edge of the vortex is defined by a higher PV value), as is typical during stratospheric warmings (O'Neill and Pope 1990). A similar shift is seen in the SH at 465 K in the runs started in November, showing the onset of the final warming at that level, At 840 K, in early November, the region of minimum dispersion disappears altogether,

suggesting that the vortex has essentially broken up at that level. The behavior at higher levels (i.e., 1100 K, 1300 K) is qualitatively similar to that at 840 K, The behavior at 420 K, the lowest level at which parcels are initialized in these simulations, is very similar qualitatively to that at 465 K. A similar picture of the extent and evolution of the vortex is obtained by examining PV dispersion.

in general, the mixing inside the vortex remains small compared to outside. However, in late winter in the SH there is a slight increase in mixing at the highest PV values in the lower stratosphere (465 K). In addition, during periods of strong wave activity, such as the stratospheric sudden warmings discussed above, and the SH final warming, the amount of mixing inside the vortex also increases. In general, there still remains a minimim in mixing along the edge of the vortex (although that edge changes it's PV position) until the final warming.

Dahlberg and Bowman (1994) examined barriers to mixing on isentropic surfaces in the NH lower stratosphere by enumerating the number of parcels crossing a PV contour. Figure 9 shows time series for parcels started at 465 and 840 K of a similar diagnostic, We show separately the number of parcels as a function of PV that are at higher and lower PV than their initial value, and the average change in PV of those parcels from their original value. Thus, if the PV value in question represents the vortex edge, the number of parcels at lower PV would represent those that had escaped from the vortex, and the number at higher PV those entrained into the vortex, The region of strong PV gradients is usually from ≈ 1.0 to 1.8×10^{-4} s^{-1}, so parcels whose PV changes by less than $\approx 0.8 \times 10\text{-}4s^{-1}$ in the vicinity of the vortex edge generally are still near the vortex edge region.

In early winter in the lower stratosphere, the parcels whose PV decreases are located mainly along the outside edge of the region of strongest PV gradients, and the parcels whose PV increases are located along the inside of the region of strongest PV gradients. There are more parcels moving to higher PV than to lower PV. During this time, the size of the vortex is increasing (i.e., the area contained within a given PV contour); the

pattern seen here suggests that diabatic effects cause the air parcels to move poleward with respect to PV, although we cannot distinguish here between poleward motion of the parcels and equatorward motion of the PV contour. In general, the PV of parcels moving both inward and outward from the vicinity of the vortex edge changes by only a small amount. This is evidence that there is little mixing between inside and outside the vortex. Those changes that are seen are consistent overall with those expected from the radiative and dynamical situation in early winter. Small changes in PV may also be caused by the low resolution and inaccuracies in calculation of the PV fields.

A similar situation is seen in early winter in the mid-stratosphere, but both the parcels increasing and decreasing in PV are mainly located toward the outside of the region of strong PV gradients. This suggests more mid-latitude mixing, as expected during the formation of the main vortex/surf zone (McIntyre and Palmer 1984) in early winter,

In late winter, the number of parcels increasing and decreasing in PV are more similar than in early winter. While in the SH, the positions of these parcels are similar to those in early winter, in the NH the region where parcels are decreasing in PV is more widespread, although it is still strongest near the region of strong PV gradients As in early winter, parcels in the SH do not change their PV by significant amounts. In the NH, a large number of parcels from inside the vortex decrease considerably in PV during March and early April. Since there are strong stratospheric warmings during this time, this suggests material being stripped off the vortex, in tongues that eventually become too narrow to be resolved in the PV fields. In the SH spring, in the lower stratosphere, and in late winter in the mid-stratosphere, parcels at the highest PV values are seen to decrease in PV by large amounts. This reflects mainly the decrease in maximum PV values, and in area enclosed by high PV contours, as radiative effects act to weaken the vortex.

While the behavior at 420 K, the lowest level at which parcels are initialized, appears qualitatively similar to that at 465 K, the plots of numbers of parcels and average

PV change become more difficult to interpret, because below 420 K, the PV scaling used here becomes increasingly inappropriate, and as the parcels descend, a given PV value is no longer representative of the same position with respect to the polar vortex. Since the behavior in the lower stratosphere is of particular interest, we examine more closely the motion of parcels initialized at 420 K. Figure 10 shows the positions of parcels started at 420 K for each of the early and late winter periods studied, initially and after 55 days; parcels are separated into those with initial PV higher and lower than a value representative of the edge of the vortex at 420 K, In early winter, parcels started at 420 K descend as far as ≈375 K (a few parcels may descend further, but have reached the boundary of the model at this point). In both NH winters, and in the SH winter of 1992, a significant number of parcels have moved away from the 420 K vortex region, and a significant number of parcels from outside this region have moved inside it In the SH 1993 early winter, no parcels appear to move significantly outside the 420 K vortex region, and only one tongue of a few parcels appears to intrude into it. In the late winter, parcels started at 420 K descend only to ≈400 Kin the same time period, In the NH, a large tongue of parcels has been drawn out of the 420 K vortex region, but most of the parcels that have moved inside the vortex region remain in the region of strong PV gradients. In the SH late winter, only a few parcels have peeled off "the edge of the vortex, and all parcels that have moved inwards remain in the region of strong PV gradients.

Figure 11 shows zonal mesh winds at a function of latitude and θ from the mid-troposphere through the lower stratosphere, at the beginning of Dec (Jun), Jan (Jul), Feb (Aug), and Mar (Sep) in the NH (SH) during the 1992 and 1993 winters. In early winter, the stratospheric polar night jet is weak at ≈400 K, and moves downward as the season progresses. In the 1992 SH winter, and in both NH winters, the polar night jet is quite weak near 400 K at the beginning of Jul (Jan); thus air parcels that descend below this level will experience little barrier to transport into mid-latitudes, or to transport from middle to higher latitudes. The strongest barrier to mixing in these cases will be the sub-

tropical jet. In the 1993 SH winter, the polar night jet strengthens and moves downward in the lower stratosphere earlier, before 1 Jul, providing a significant barrier to transport even in early winter. The polar night jet in the NH lower stratosphere in early winter 1993 is considerably weaker than in 1992, and, consistent with this, there is more mixing between polar and mid-latitude air in 1993.

Figure 12 shows the 375 K PV fields in the middle of each of the time periods. Consistent with the zonal mean picture shown above, in early winter, between 420 K and 375 K, PV gradients shift from strongest around the polar vortex to relatively weak gradients in the polar regions and strongest gradients in the subtropics, In late winter, strong gradients are apparent both in the polar and sub-tropical regions.

It is apparent from the above discussion that the amount of descent in the lower stratosphere is critical, especially in early winter, to determining whether air can move from the polar regions into mid-latitudes. In late winter, parcels descend less, and not many of the parcels in this simulation move below ≈400 K. In addition, the polar night jet moves downwards, so that even as far down as 375 K, strong PV gradients in the polar regions present a barrier to mixing. In the NH late winter, these gradients are weaker than in the SH, and some material is seen being stripped away into mid-latitudes; the NH PV fields themselves are also more distorted, which may result in the appearance of more air escaping from the vortex, as filaments of high PV drawn off the vortex become too narrow to resolve.

Figure 13 shows the zonal mean winds in the SH at the beginning of October and November in 1992 and 1993, Although the polar night jet is weakening, relatively strong winds still extend below 375 K. Figure 14 shows the positions in late November of parcels started at 420 K in mid-August. As expected from the winds, most parcels remain separated by their original location with respect to the vortex. Figure 15 shows the positions of parcels initialized in early November at 420 K, in mid-December. Despite the lateness of the spring season, at this level near the bottom of the stratosphere,

most of the parcels that were initially inside the polar vortex region remain confined there, consistent with the strong PV gradients still apparent. Although a few parcels have escaped to middle and low latitudes, these represent less than 10% of the parcels initially in the vortex region.

5. The Final Warming

Figure 16 shows a series of 3-d perspectives of the positions of parcels initialized in mid-August in the SH in the two years studied, inside the 1.2 x 10^{-4} s^{-1} scaled PV contour. The dates shown are in November and December, when parcels started in the upper stratosphere have descended to the mid-stratosphere, and the vortex is breaking up in the mid-stratosphere. Figure 17 shows sequences of figures on the same dates, but with parcels initialized in early November, so the behavior is shown to higher levels. The process of the vortex break up in the mid-stratosphere is dramatically illustrated. In both years the break up is characterized by large, relatively deep tongues of material being stripped off the vortex, and drawn out into low latitudes. These tongues, or vortex fragments, frequently maintain their identity for days to weeks.

During both years, the SH final warming was relatively late, and therefore, controlled to a large extent by radiative processes. As noted earlier, throughout the 1993 SH winter there was less wave activity than in the 1992 winter. The sequences shown indicate, consistent with this, that the final warming is less advanced cm the same date in 1993 than in 1992. In the NH, where wave activity is typically much stronger throughout the winter, the final warming is usually much earlier and is dynamically induced (e.g., O'Neil] and Pope 1990); this was the case during 1993 (Manney et al. 1994 b), Figure 18 shows 3-d perspectives of parcel positions in March and April 1992, similar to those shown for the SH. At this time, the scaled PV isosurface that is shown (1,2 x 10-4 s^{-1}) is no longer representative of the vortex edge (see Fig. 8). Although the process of the

breakup is still characterized by large tongues of air being drawn off the vortex, in the middle and upper stratosphere the process is faster and begins when the vortex is already eroded and distorted by earlier warmings; by the end of this simulation, the parcels initialized in the upper levels appear randomized.

In the previous section it was shown that at 420 K, the vortex remains fundamentally intact into December in the SH and into April in the NH, well after it has broken up in the mid-stratosphere. Figure 19 summarizes the behavior of parcels started at levels from 465 K through 655 K during the final warming, showing a projection on a horizontal plane of the positions of those parcels started within the $1.2 \times 10^{-4}\ s^{-1}$ scaled PV contour in early November, color coded by their starting level. By mid-December in the SH, many parcels started at 655 K and 585 K have been stripped away from the vortex, while at the lower levels, 520 K and 465 K, the majority of parcels are still confined. The case is similar in April in the NH, but the parcels at 655 K and 585 K are more randomized than their SH counterparts, and more of those in the lowest levels have been stripped away from the vortex.

6. **Discussion and Conclusions**

Trajectory calculations using horizontal winds from a data assimilation analysis, and vertical velocities calculated by a middle atmosphere radiation scheme are used to diagnose characteristics of air motion for both early and late winter time periods in the northern and southern hemispheres. As expected, the net air motion is polewards and downwards throughout the winter.

The strongest overall diabatic descent in the SH is in the center of the polar vortex at levels above ≈900 K, and near the edge of the vortex below this level. In the lower stratosphere, below ≈600 K, the strongest descent is along the outside edge of the vortex. In the NH, a similar pattern of descent is seen in late winter, with strongest descent on the

edge of the vortex extending higher in the stratosphere during times of particularly strong wave activity, consistent with observations of strongest diabatic cooling between the polar vortex and the anti-cyclone during stratospheric warmings. In contrast, in early winter in the NH, strongest descent is usually near the center of the vortex. The patterns of descent in the late winter lower stratosphere are consistent with those shown by Schoeberl et al. (1992), In the SH, parcels in the lower stratosphere cease to descend in mid-October, although even in November, parcels in the mid-stratosphere polar regions still experience some descent, However, the uncertainties in magnitude and even sign of the computed heating rates are relatively large when the rates are small, so the exact time of changes from descent to ascent is uncertain. Rough estimates of geometrical vertical velocities and of diabatic descent computed here are generally consistent with estimates given by Schoeberl et al, (1992) and Strahan et al. (1994) for earlier years and with recent estimates using UARS passive tracer data (Santee et al. 1994, paper in preparation) and radiative inputs (Eluszkiewicz et al. 1994, this issue).

Diagnostics of mixing show a strong barrier to mixing at the edge of the polar vortex in the lower stratosphere, even into December in the SH. In the middle stratosphere, stratospheric warmings cause mixing to increase, and the vortex edge, as identified by a minimum in mixing, to move to higher PV values. This is consistent with previous studies showing the shrinking of the vortex and weakening of PV gradients during stratospheric warmings. As expected, considerably more mixing is seen in the NH than in the SH. In the lower stratosphere, in early winter the polar night jet usually does not extend significantly below ≈400 K, and parcels that descend below this level experience little barrier to mixing into mid-latitudes. As the winter progresses, the polar night jet moves downwards, and the parcels descend more slowly. Consistent with this, our simulations show considerably less mixing of polar air into mid-latitudes in late winter than in early winter in both hemispheres. In the presence of this polar night jet structure in the lower stratosphere and the sub-tropical jet in the upper troposphere, the degree of mixing

between polar and mid-latitude air in the lower stratosphere is strongly dependent on the amount of descent. Unfortunately, our quantitative knowledge of these rates is still limited.

Computed radiative heating rates are still sensitive to the sophistication of the radiative transfer codes (e.g., the number of vertical levels used or the treatment of line shape and overlap) and to the fields required as input, especially ozone and temperature. This is particularly true outside the polar night, when the net rates are often the sum of two large, opposing terms. As noted earlier, the net heating rates are likely to be most uncertain when they are small. The descent rates computed here produce tracer motions that agree fairly well with UARS observations of the long-lived tracers N_2O and CH_4 (Manney et al. 1994d, this issue). This suggests therefore, that actual diabatic descent rates in the lower stratosphere are closer to the lower values diagnosed by Hartmann et al. (1989) and Schoeberl et al. (1992) than to those suggested, for example, by Proffitt et al. (1 992).

A three-dimensional picture has been drawn of the final warming in the stratosphere. The breakup of the polar vortex is characterized by large fragments of polar air being stripped from the vortex and drawn out into increasingly narrow tongues in low latitudes. In the SH, this process is relatively slow, and these fragments may maintain their identity for weeks; in the NH, the final warming is dynamically induced, and is more rapid, with parcels from the mid-stratospheric polar vortex being spread throughout the hemisphere by early April in the year shown here. The large degree of interannual variability in the NH late winter suggests that many variations on this behavior might be observed during other years, For the period of UARS observations, the vortex in the lower stratosphere remains intact, and many of the air parcels confined within it, into December in the SH, and into April in the NH, well after the vortex has broken up in the mid-stratosphere.

Acknowledgments. We thanks our MLS colleagues for their continued collaboration and support; T. Luu for data management; P. A. Newman for routines that were adapted

to calculate PV, W. J. Randel for helpful discussions. This research was sponsored by NASA's Upper Atmosphere Research Satellite Project and was performed at the Jet Propulsion Laboratory, California Institute of Technology under contract with the National Aeronautics and Space Administration.

References

Bowman, K. P., 1993a: Barotropic simulation of large-scale mixing in the Antarctic polar vortex, *J. Atmos. Sci., 50, 2901-2914.*

Bowman, K. P., 1993b: Large-scale isentropic mixing properties of the Antarctic polar vortex from analyzed winds, *J. Geophys. Res.*, **98, 23,013-23,027.**

Bowman, K. P., and P. Chen, 1994: Mixing by barotropic instability in a non-linear model, *J. Atmos. Sci.,* submitted.

Chen, P., 1994: The permeability of the Antarctic vortex edge, *J. Geophys. Res.,* submitted.

Chen, P., and J. R. Holton, 1994: Transport of conserved tracers by unstable barotropic waves, *J. Atmos. Sci.,* submitted.

Chen, P., J. R. Holton, A. O'Neill, and R. Swinbank, 1994: Quasi-horizontal transport and mixing in the Antarctic stratosphere, *J. Geophys. Res.,* submitted.

Dahlberg, S. P., and K. P. Bowman, 1994: Climatology of large-scale isentropic mixing in the Arctic winter stratosphere from analyzed winds, *J. Geophys. Res.,* submitted,

Dunkerton, T. J., and D. P. Delisi, 1986: Evolution of potential vorticity in the winter stratosphere of January-February, 1979. *J. Geophys. Res.,* **91, 1199-1208.**

Fishbein, E. F., L. S. Elson. L. Froidevaux, G. L. Manney, W. G. Read, J. W. Waters, and R. W. Zurek, 1993: MLS observations of stratospheric waves in temperature and O_3 during the 1992 southern winter. *Geophys. Res. Lett.,* 20, 1255-1258.

Fisher, M., A. O'Neill, and R. Sutton, 1993: Rapid Descent of Mesospheric Air in the Stratospheric Polar Vortex. *Geophys. Res. Lett.,* **20, 1267-1270.**

Hartmann, D. L., L. E. Heidt, M. Loewenstein, J. R. Podolske, J. Vedder, W. L. Starr, and S. E. Strahan, 1989: Transport into the South polar vortex in early spring, *J. Geophys. Res.,* 94,16,779-16,796.

Manney, G. L., and R. W. Zurek, 1993: Interhemispheric comparison of the development of the stratospheric polar vortex during fall: A 3-dimensional perspective for 1991-1992, *Geophys. Res. Lett., 20, 1275-1278.*

Manney, G. L., L. Froidevaux, J. W. Waters, L. S. Elson, E. F. Fishbein, R. W. Zurek, R. S. Harwood, and W. A. Lahoz, 1993: The evolution of ozone observed by UARS MLS in the 1992 late winter southern polar vortex. *Geophys. Res. Lett.,* 20, 1279-1282.

Manney, G. L., J. D. Farrara, and C. R. Mechoso, 1994a: Simulations of the February 1979 stratospheric sudden warming: Mode] comparisons and Three-dimensional evolution, *Mon. Wea. Rev.,* in press.

Manney, G. L., R. W. Zurek, A. O'Neil], R. Swinbank, J. B. Kumer, J. L. Mergenthaler, and A. E. Roche, 1994b: Stratospheric Warmings during February and March 1993. *Geophys. Res. Lett.,* in press.

Manney, G, L., L. Froidevaux, J. W. Waters, R, W. Zurek, W. G. Read, L. S. Elson, J. B. Kumer, J. L. Mergenthaler, A. E. Roche, A. O'Neill, R. S. Harwood, I. MacKenzie, and R. Swinbank, 1994c: Chemical depletion of lower stratospheric ozone in the 1992-1993 northern winter vortex, *Nature,* submitted.

Manney, G. L., W. A. Lahoz, R. S. Harwood, R. W. Zurek, J. B. Kumer, J. L. Mergenthaler, A. E. Roche, A. O'Neill, R. Swinbank, and J. W. Waters, 1994d: Lagrangian transport calculations using UARS data. Part I: Passive tracers, *J. Amos. Sci.,* submitted (this issue).

McIntyre, M. E., 1989: On the Antarctic ozone hole, *J. Amos. Terr. Phys.,* **51,29-43.**

McIntyre, M. E., and T. N. Palmer, 1984: The 'surf zone' in the stratosphere, *J. Atmos. Terr. Phys., 46,825-849.*

Morris, G. A., M. R. Schoeberl, L. Sparling, P. A. Newman, L. R. Lait, L. S. Elson, J. W. Waters, A. E. Roche, J. B. Kumer, and J. M. Russell, 111, 1994: Trajectory mapping

of Upper Atmosphere Research Satellite (UARS) data, *J. Geophys. Res.*, submitted.

O'Neill, A., and V. D. Pope, 1990: The seasonal evolution of the extra-tropical stratosphere in the southern and northern hemispheres: Systematic changes in potential vorticity and the non-conservative effects of radiation, *Dynamics, Transport and Photochemistry in the Middle Atmosphere of the Southern Hemisphere, 33-54,* Kluwer Academic Publishers, Netherlands.

Pierce, R. B., and T. D. A. Fairlie, 1993: Chaotic advection in the stratosphere: Implications for the dispersal of chemically perturbed air from the polar vortex, *J. Geophys. Res., 98,* 18,589-18,595.

Plumb, R. A., D. W. Waugh, R. J. Atkinson, P. A. Newman, L. R. Lait, M. R. Schoeberl, E. V. Browell, A. J. Simmons, and M. Loewenstein, 1994: Intrusions into the lower stratospheric Arctic vortex during the winter of 1991-1992, *J. Geophys. Res.,* 99, 1089-1105.

Proffitt, M. H., K. K. Kelly, J. A. Powell, B. L. Gary, M. Loewenstein, J. R. Podolske, S. E. Strahan, and K. R. Chan, 1989: Evidence of diabatic cooling and poleward transport within and around the 1987 Antarctic ozone hole, *J. Geophys. Res., 94, 16,797-16,814.*

Proffitt, M. H., J. J. Margitan, K. K. Kelly, M, Loewenstein, J. R. Podolske, and K. R. Chan, 1992: Ozone loss in the Arctic polar vortex inferred from high-altitude aircraft measurements, *Nature, 347, 31-36, 1992.*

Randel, W. J., 1993: Ideas flow on Antarctic vortex. *Nature,* 364, 105-106.

Russell, J. M. 111, A. F. Tuck, L. F. Gordley, J. H. Park, S. R. Drayson, J. E. Harries, R. J. Cicerone, and P. J. Crutzen, 1993: HALOE Antarctic observations in the spring of 1991, *Geophys. Res. Lett., 20,719-722.*

Schoeberl, M. R., L. R. Lait, P, A, Newman, R. L. Martin, M. H. Proffitt, D. L. Hartmann, M. Loewenstein, J, Podolske, S. E. Strahan, J. Anderson, K. R, Chan, and B.

L. Gary, 1989: Reconstruction of the constituent distribution and trends in the Antarctic polar vortex from ER-2 flight observations, *J. Geophys. Res.*, 94, 16,815-16,846.

Schoeberl, M. R., L. R. Lait. P. A. Newman, and J. E. Rosenfield, 1992: The structure of the polar vortex. *J. Geophys. Res., 97,7859-7882.*

Shine, K. P., 1987: The middle atmosphere in the absence of dynamic heat fluxes. *Quart. J. Roy. Meteor. Sot.,* **113,603-633.**

Strahan, S. E., J. E, Rosenfield, M. Loewenstein, J. R. Podolske, and A. Weaver, 1994: The evolution of the 1991-2 Arctic vortex and comparison with the GFDL ' SKYHI' general circulation model, *J. Geophys. Res.,* submitted.

Swinbank, R., and A, O'Neil], 1994: A Stratosphere-troposphere data assimilation system, *Mon. Wea. Rev.,* **122,686-702.**

Tuck, A. F., 1989: Synoptic and chemical evolution of the Antarctic vortex in late winter and early spring, 1987, *J. Geophys. Res.*, 94, 11,687-11,737.

Tuck, A. F., T. Davies, S. J. Hovde, M. Noguer-Alba, D. W. Fahey, S. R. Kawa, K. K. Kelly, D. M. Murphy, M. H. Proffitt, J. J, Margitan, M. Loewenstein, J. R, Podolske, S. E. Strahan, and K, R. Chan, 1992: Polar stratospheric cloud processed air and potential vorticity in the Northern Hemisphere lower stratosphere at mid-latitudes during winter, *J. Geophys. Res.,* 97,7883-7904.

Tuck, A. F., J. M. Russell III, and J. E. Harries, 1993: Stratospheric Dryness: Antiphased desiccation over Micronesia and Antarctica, *Geophys. Res. Lett., 20, 1227-1230,*

Waugh, D. W., R. A. Plumb, R. J. Atkinson, M. R. Schoeberl, L. R. Lait, P. A. Newman, M .Loewenstein, D. W. Toohey, L. M. Avallone, C. R. Webster, and R. D. May, 1994: Transport out of the lower stratospheric Arctic vortex by Rossby wave breaking, *J. Geophys. Res.,* 99, 1071-1088.

TABLE 1: PERIODS COVERED BY TRAJECTORY CALCULATIONS

SEASON	SOUTHERN HEMISPHERE	NORTHERN HEMISPHERE
EARLY WINTER	1 June -6 August 1992 1 June -6 August 1993	1 Dec 1992 - 5 Feb 1993 1 Dec 1993-5 Feb 1994
LATE WINTER - SPRING	17 August -16 Dec 1992 9 August -19 Dec 1993	12 Feb -8 April 1993 -------
SPRING (Re-initialized)	2 Nov - 16 Dec 1992 1 Nov - 15 Dec 1993	-------

Table 2. Estimates of geometrical vertical velocity from Fig. 2. Vertical velocities are given to one significant figure, and estimates are included near the pole, and at the location of maximum downward velocity. For Feb 1993, only the maximum velocity is estimated, due to the large spread in parcel positions. Positive values indicate *downward* motion.

start alt(s) (km)	end alt(s) (km)		vrt vel (cm/s)	
	pole	minimum	pole	maximum
NH Dec 92				
47	32	32	0.3	0.3
39-44	29-31	29-31	0.2	0.2
37	28.5	27,5	0.1	0,2
34	28	26	0.1	0.1
29-31	24-26	22-24	0.09	0.1
25	23	20	0.04	0,09
22	21	18	0.02	0.07
19	18,5	16	0.009	0.05
17	16	13	0.02	0.07
SH Jun 92				
43-47	33-34	33-34	0.2	0.2
37-39	31-32	26-28	0.1	0.2
35	31	27	0.07	0.1
33	30	25	0.05	0.1
28-30	26-28	20-22	0.03	0.1
25	23	18	0.04	0.1
21	20	16	0.02	0.09
18	18	13	0	0.09
NH Feb 93				
47		32		0.3
37-43		29-31		0$2
32-35		26-28		0.1
25-29		21-25		0.08
22		18		0.07
17-20		14-17		0.06
SH Aug 92				
43-46	31-32	30-31	0.3	0.3
38-41	30-31	29-30	0.2	0.2
3 6	30	28	0.1	0.2
32-34	27-29	25-27	0.1	0.1
26-30	22-26	19-23	0.08	0.1
23	20	16	0.6	0.1
20	19	13	0.03	0.1

Table 3. Estimates of average diabatic descent for several isentropic surfaces. The maximum descent seen or parcels averaged in PV bins (see text) is given, along with the scaled PV (10^{-4} s^{-1}) at which that maximum occurred. "Center" indicates the maximum occurred at the highest PV values present. The vortex edge is typically from ≈1.0 to 1.4 x 10^{-4} s^{-1} in the scaled units used here.

start (K)	season	NH/SH	position	$d\theta/dt$ (K/d)
1300 K	EW	NH	center	9.5
		SH	center	9.5
	LW	NH	center	9.0
		SH	center	8.8
	SPR	SH	???	1 to 3
840 K	EW	NH	center	3.6
		SH	center	3.0
	LW	NH	center	3.6
		SH	PV=1.2	2.5
	SPR	SH	center	2 to 3
465 K	EW	NH	center	0.8
		SH	PV=1.2	0.7
	LW	NH	PV=1.4	0.5
		SH	PV=1.0	0.4
	SPR	SH	PV=1.2	0.3
420 K	EW	NH	center	0.6
		SH	PV=1.0	0.6
	LW	NH	PV=1.0	0.4
		SH	PV=0.9	0.4
	SPR	SH	PV=1.2	0.2

Figure Captions

Figure 1. Cross-sections in potential temperature (θ) and latitude of the positions of parcels, 66 days after the beginning of runs started in early winter (a through d) and 55 days after the beginning of runs started in late winter (e through g). Parcels are color-coded by their initial level; initial levels are indicated by colored lines on the figures.

Figure 2. Cross-sections in pressure and latitude of the positions of parcels, O and 66 days after the beginning of runs started in early winter (a through d) and O and 55 days after the beginning of runs started in late winter (e through h). Parcels are color-coded by their initial level, those levels being the same as indicated in Fig. 1. The vertical coordinate is pressure altitude, computed as (7 km)·log([1000 hPa]/p).

Figure 3. Cross-sections in potential temperature (θ) and latitude of the positions of parcels, 110 days after the beginning of runs started in late winter in the SH (a and b) and 33 days after the beginning of runs started in spring in the SH (c and d). Parcels are color-coded by their initial level; initial levels are indicated by colored lines on the figures,

Figure 4. Potential temperature (θ, K) of parcels started in early winter on the 1100, 840, and 465 K isentropes, 55 days after the beginning of the runs. The color bar for all plots from a given level is at the beginning of that row.

Figure 5. As in Fig, 4, but for late winter runs.

Figure 6. As in Fig. 4, but 110 days after the beginning of the late winter runs.

Figure 7. Time series of the average change in potential temperature (K) of parcels divided into bins by their initial scaled potential vorticity (PV), as a function of initial scaled PV (-PV in the SH). Bins are 0.2 x 10^{-4} s^{-1} wide, centered around the values at the tick marks. Time series for early and late winter runs are 55 days long;

those for SH spring runs are 44 days long,

Figure 8. Time series of the latitude dispersion (degrees^2) of parcels divided into bins by their initial scaled potential vorticity (PV), as a function of initial scaled PV (-PV in the SH). Bins are 0.2 x 10-4 s^{-1} wide, centered around the values at the tick marks. Time series for early and late winter runs are 55 days long; those for SH spring runs are 44 days long.

Figure 9. Time series of the number of parcels moving to higher/lower scaled PV values, and of-the average scaled PV change (10^{-4} s^{-1}) of those parcels, as a function of their initial scaled PV (-PV in the SH). Time series for early and late winter runs are 55 days long; those for SH spring runs are 44 days long. Blank areas in the interior of plots indicate that no parcels have passed that PV contour in the plotted direction. Only the plots for parcels moving to lower PV are shown in the spring cases, since < 50 parcels move towards higher PV at that time across any contour.

Figure 10. Horizontal positions of parcels started at 420 K, for runs started in early and late winter, O and 55 days after the beginning of the runs. Parcels are separated into two groups, initially inside and outside a PV contour representative of the edge of the vortex at 420 K (outside of shading on figure panels). Parcels are color coded by their potential temperature (θ, K). Several 420 K PV contours are superimposed on each plot.

Figure 11. Zonal mean winds (m/s) as a function of latitude" and θ at the beginning of Dec (Jun), Jan (Jul), Feb (Aug) and Mar (Sep) in the NH (SH) for the 1992 and 1993 winters. Theta runs from 300 K (mid-troposphere, ≈500 hPa) to 655 K (lower middle stratosphere, ≈20 hPa). Contour interval is 4 m/s, with 28-32 m/s shaded,

Figure 12. 375 K PV (10-4 K m^2 kg^{-1} s^{-1}) 27 days after the beginning of each of the early and late winter runs. Contours run from 0.03 to 0.14 x 10-4 K m^2 kg^{-1} s^{-1}, with a contour interval of 0.01 x 10-4 K m^2 kg^{-1} s^{-1}, and shading between 0.10 and 0.11 x10^{-4} K m^2 kg^{-1} s-l; values are the negative of this in the SH.

Figure 13. As in Fig. 11, but for the beginning of Oct and Nov in the Sh in 1992 and 1993,

Figure 14. As in Fig. 10, but 99 days after the beginning of the late winter runs,

Figure 15. As in Fig. 10, but 44 days after the beginning of the runs started in Nov in the SH.

Figure 16. Three-dimensional perspectives of the positions of air parcels that were initially within the 1.2×10^{-4} s^{-1} scaled PV contour (-PV in the SH). Parcels are color coded by their initial level, with voilet representing those that started at 420 K, and dark red those that started at 1700 K. 40°,60°, and 80^{o} latitude circles are shown, and the bounding box runs from 375 K to 1700 K. The translucent white surface is the 1.2 x 10-4s- [1] scaled PV isosurface (-PV in the SH) on the plotted day. Plots are shown at 3 day intervals during the 1992 and 1993 SH final warmings, from runs started in August.

Figure 17. As in Fig. 16, but for runs started in early November in the SH.

Figure 18. As in Fig. 16, but for the run started on 10 Feb 1993 in the NH, and shown at 10 day intervals,

Figure 19. Horizontal positions of parcels started within the 1.2x 10-4s- [1] scaled PV contour (-PV in the SH) on the 465 K (violet parcels), 520 K (blue parcels), 585 K (green parcels) and 655 K (red parcels) isentropes. Parcels are shown from the runs started in Nov 1992 and 1993 in the SH, and Feb 1993 in the NH.

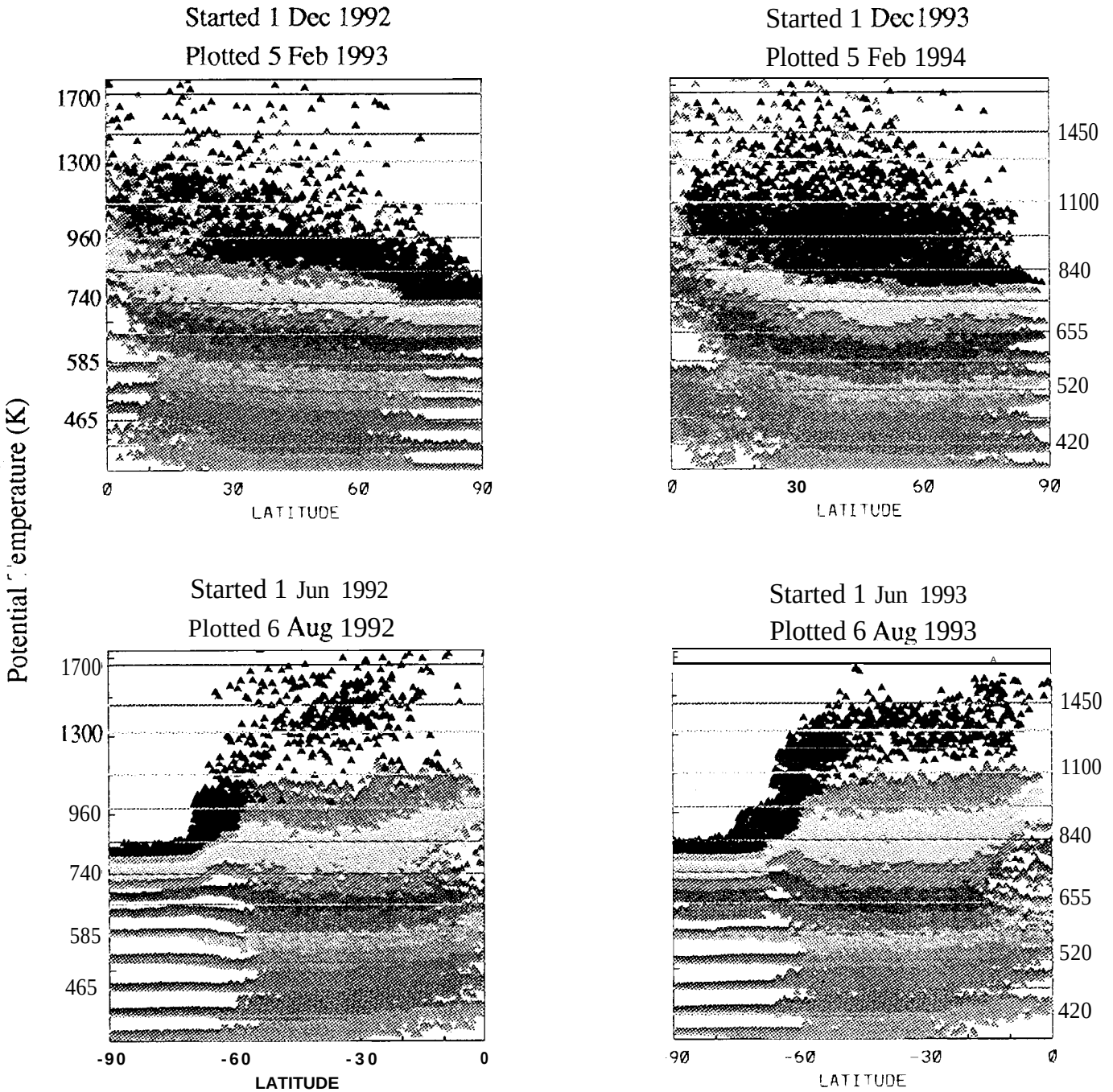
Started 1 Dec 1992
Plotted 5 Feb 1993
Started 1 Dec 1993
Plotted 5 Feb 1994
Started 1 Jun 1992
Plotted 6 Aug 1992
Started 1 Jun 1993
Plotted 6 Aug 1993
Potential Temperature (K)
1700
1300
960
740
585
465
1450
1100
840
655
520
420
0
30
60
90
-90
-60
-30
LATITUDE

Fig. 1 (a-d)

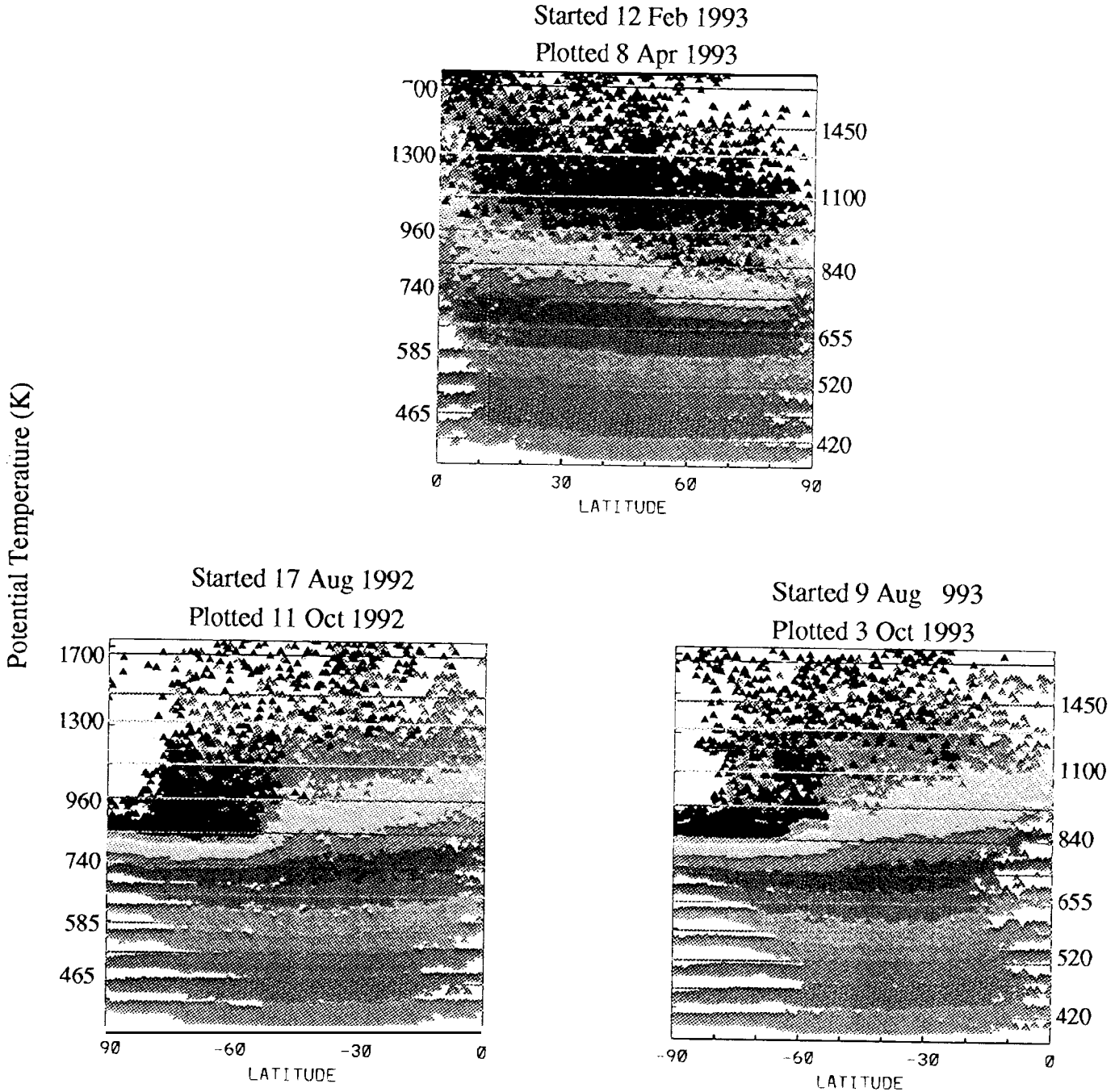
Started 12 Feb 1993
Plotted 8 Apr 1993
1300
960
740
585
465
1450
1100
840
655
520
420
0
30
60
90
LATITUDE
Started 17 Aug 1992
Plotted 11 Oct 1992
1700
1300
960
740
585
465
90
-60
-30
0
LATITUDE
Started 9 Aug 993
Plotted 3 Oct 1993
1450
1100
840
655
520
420
-90
-60
-30
0
LATITUDE
Potential Temperature (K)

Fig. 1 (e-g)

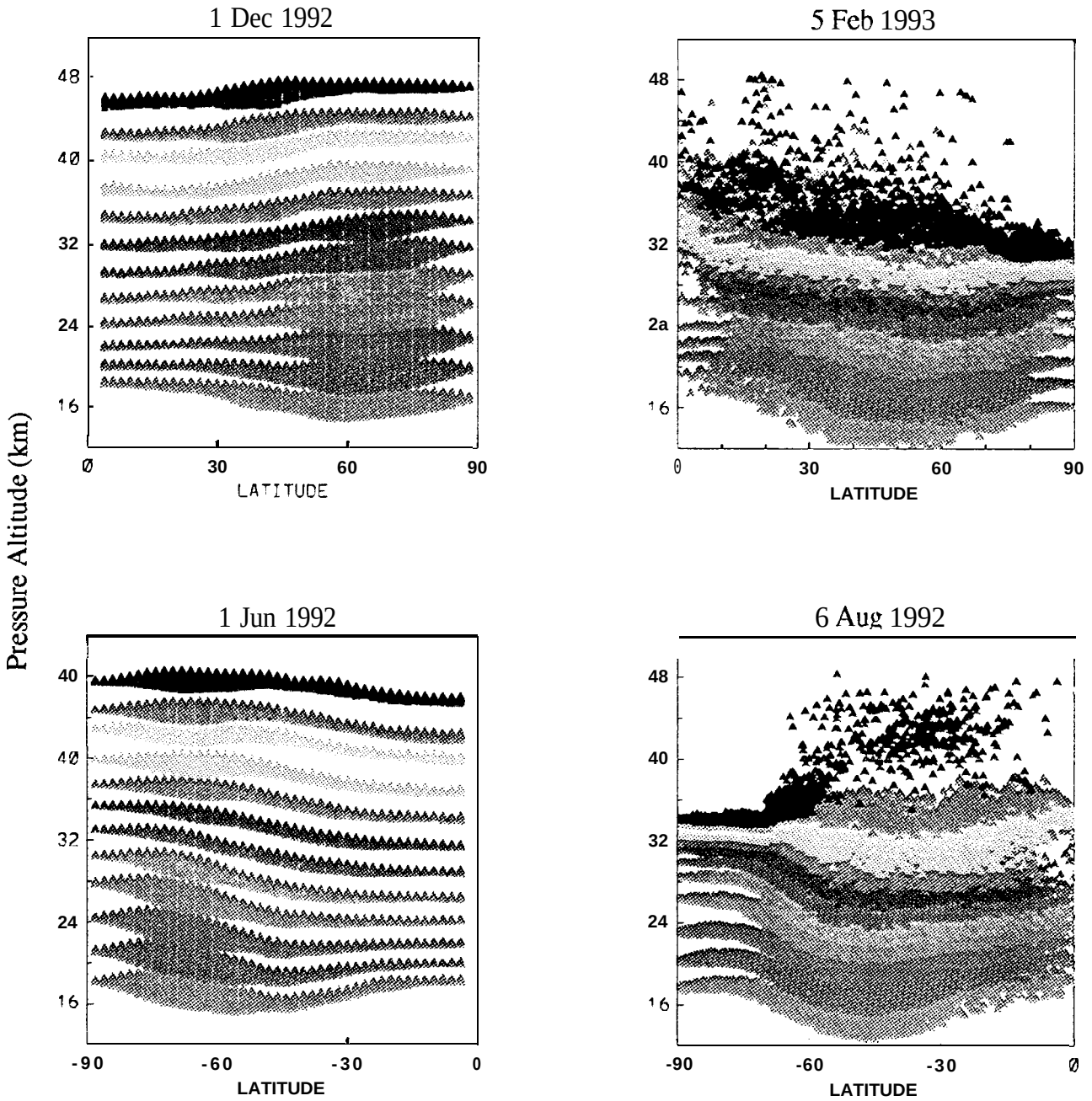
1 Dec 1992
5 Feb 1993
1 Jun 1992
6 Aug 1992
Pressure Altitude (km)
48
40
32
24
16
2a
Ø
30
60
90
-90
-60
-30
0
LATITUDE

Fig. 2 (a-d)

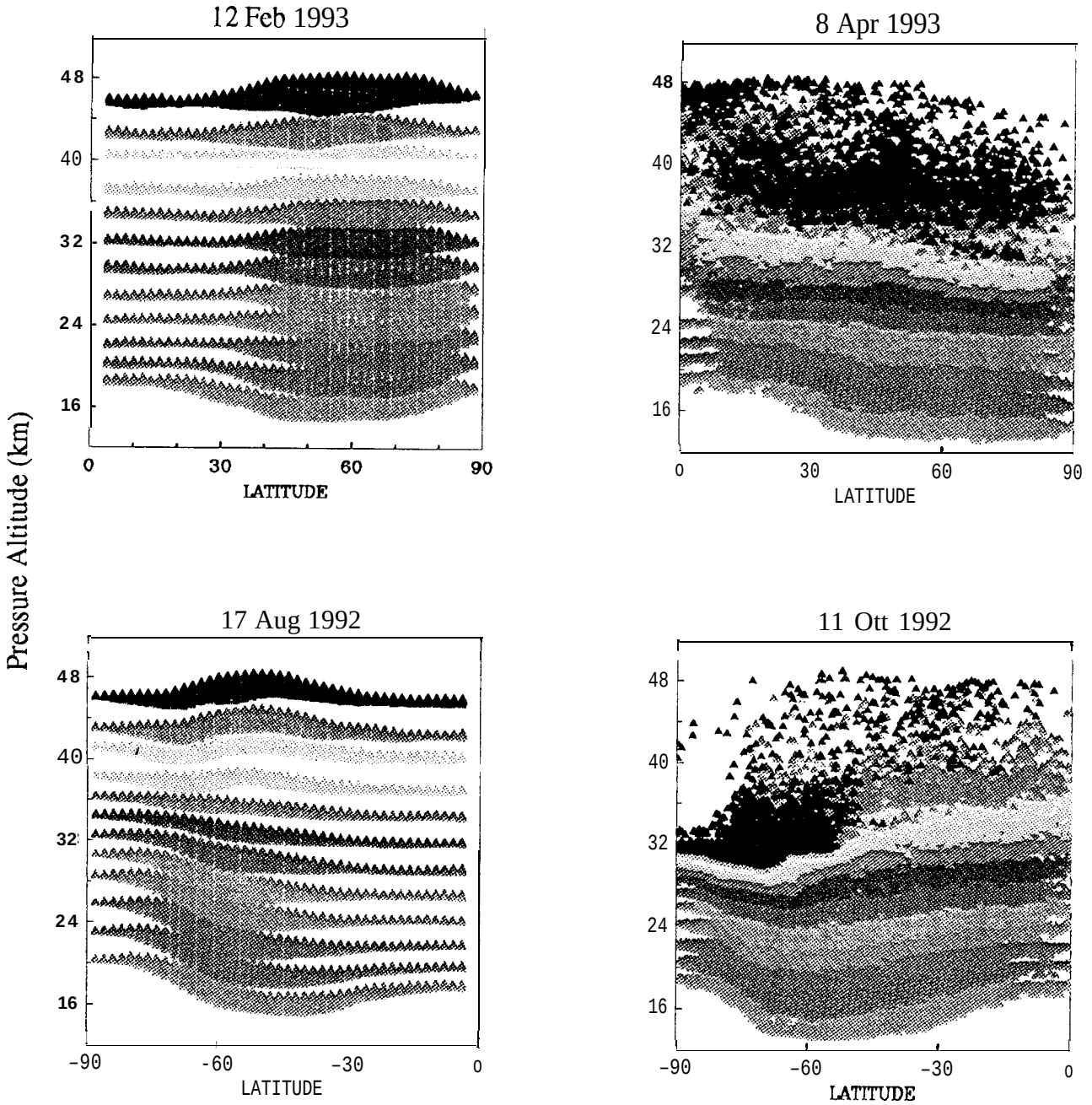
12 Feb 1993
8 Apr 1993
17 Aug 1992
11 Ott 1992
Pressure Altitude (km)
48
40
32
24
16
0
30
60
90
-90
-60
-30
LATITUDE

Fig. 2 (e-h)

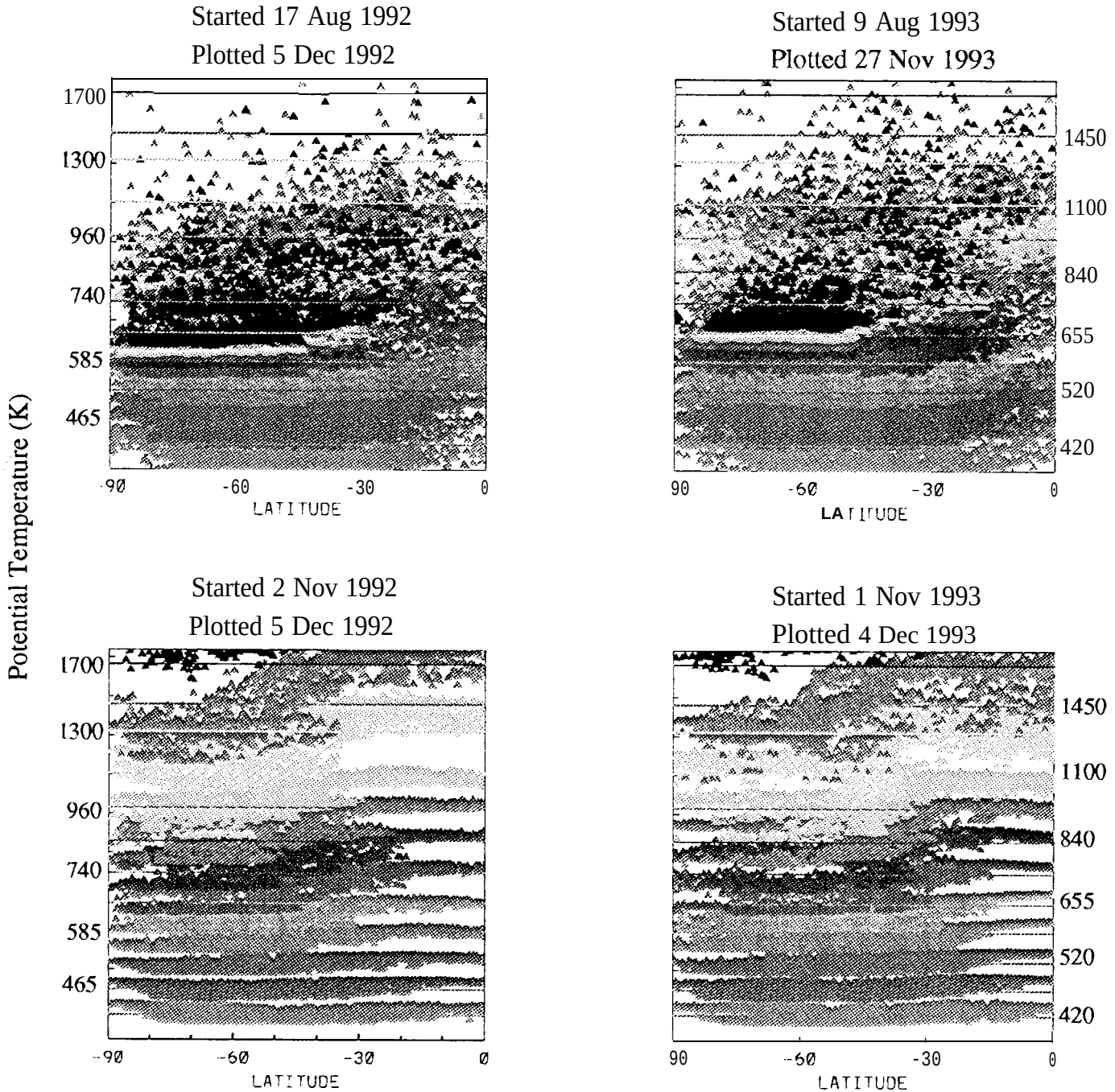
Started 17 Aug 1992
Plotted 5 Dec 1992
Started 9 Aug 1993
Plotted 27 Nov 1993
Started 2 Nov 1992
Plotted 5 Dec 1992
Started 1 Nov 1993
Plotted 4 Dec 1993
Potential Temperature (K)
1700
1300
960
740
585
465
1450
1100
840
655
520
420
-90
-60
-30
0
90
LATITUDE

Fig. 3

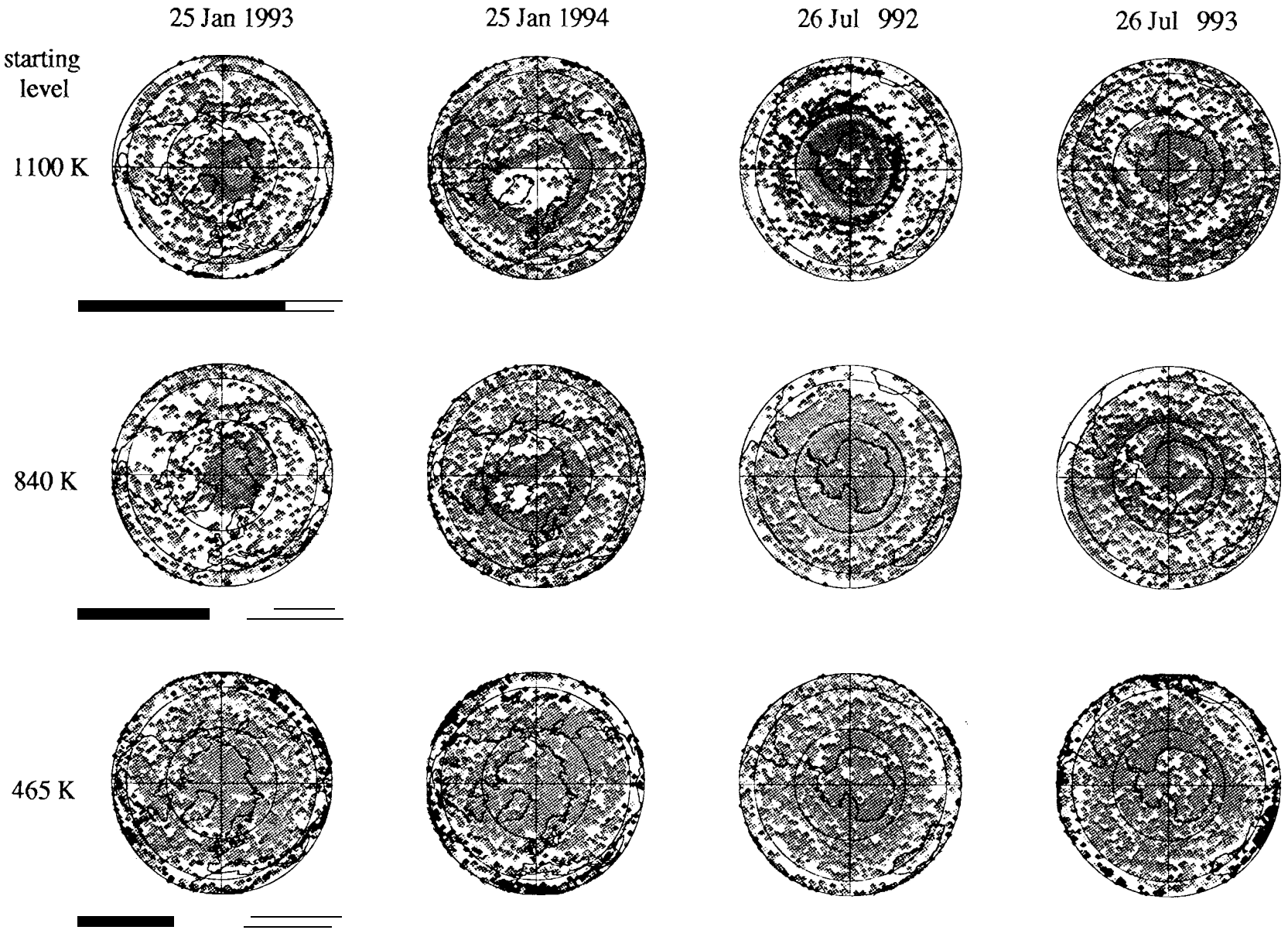
25 Jan 1993
25 Jan 1994
26 Jul 992
26 Jul 993
starting level
1100 K
840 K
465 K

Fig. 4

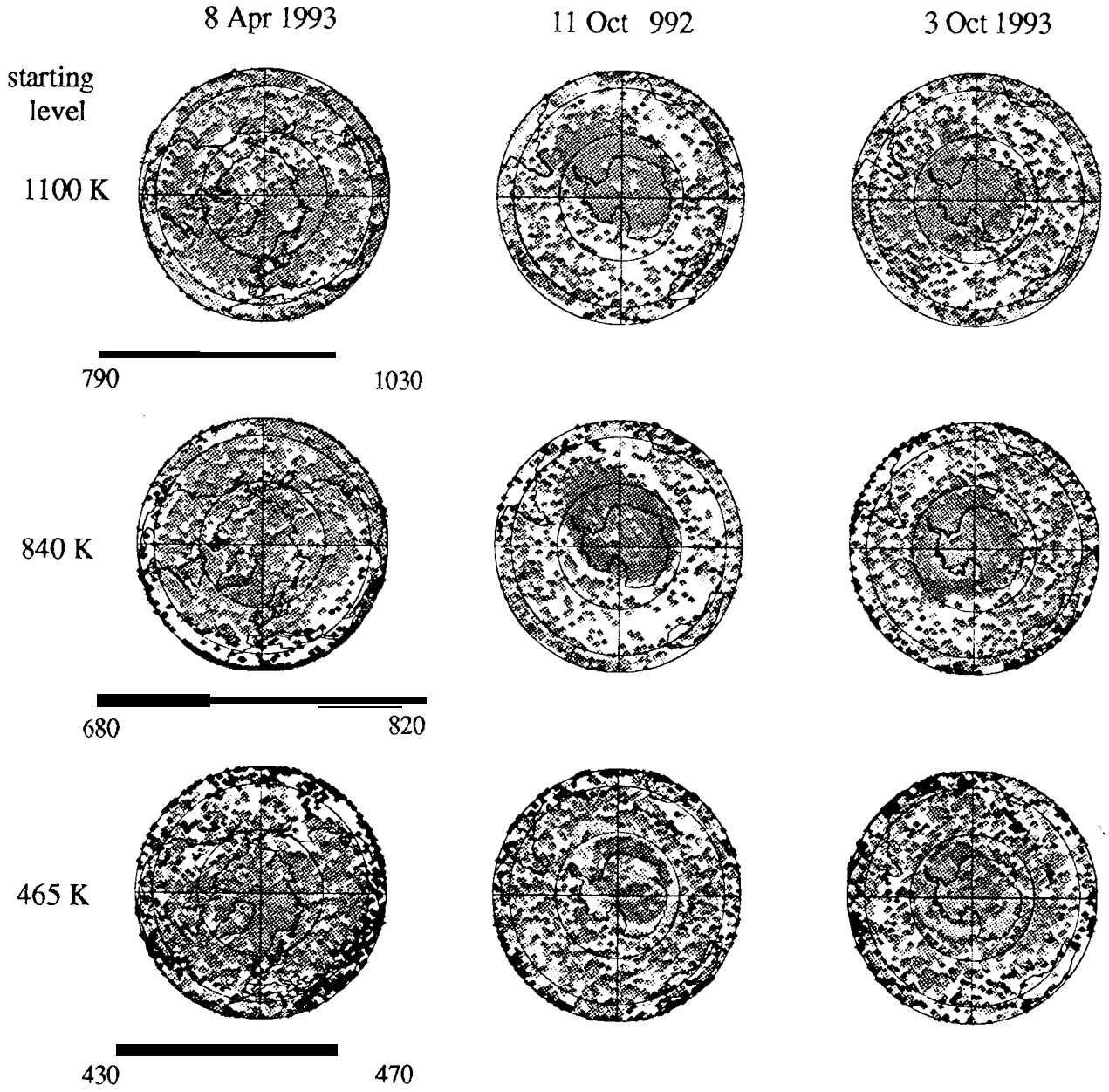
8 Apr 1993
11 Oct 992
3 Oct 1993
starting level
1100 K
790
1030
840 K
680
820
465 K
430
470

Fig. 5

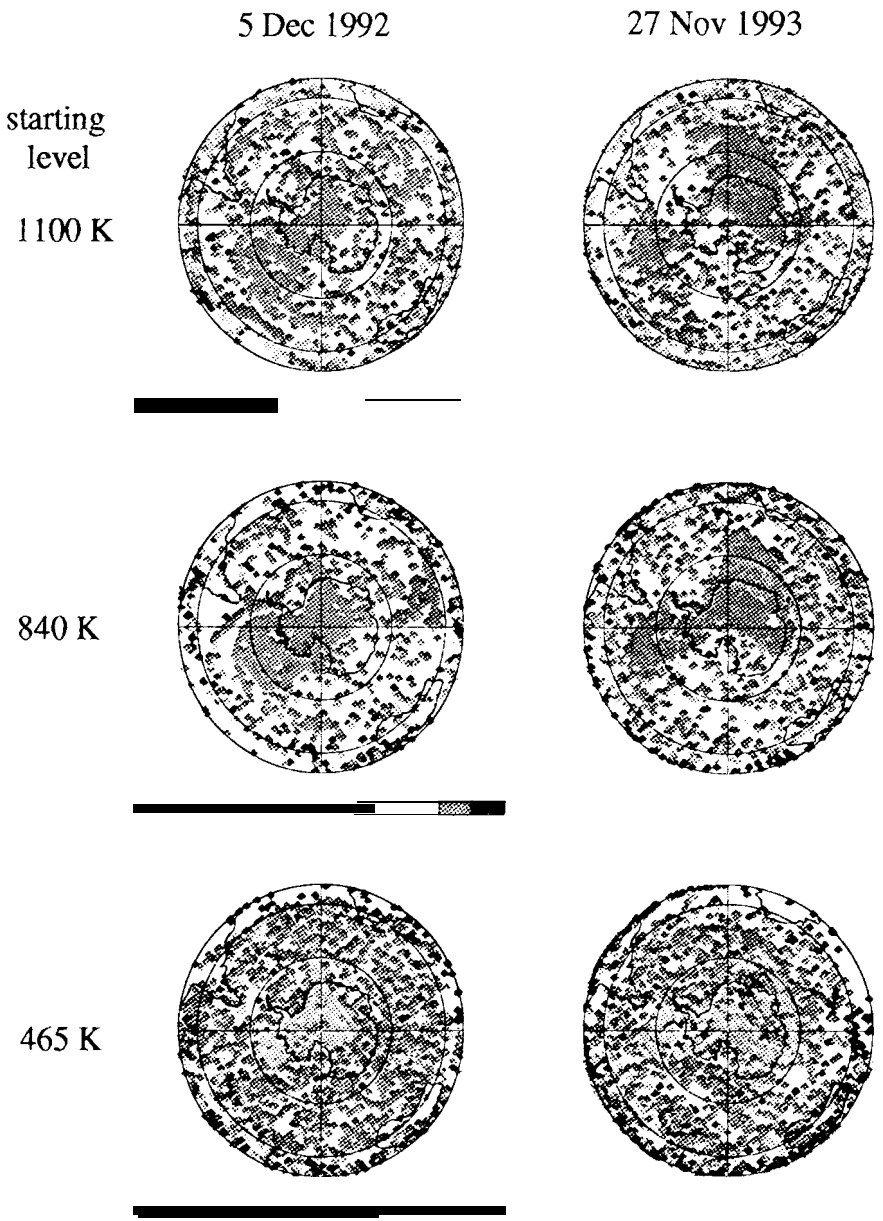

Fig. 6

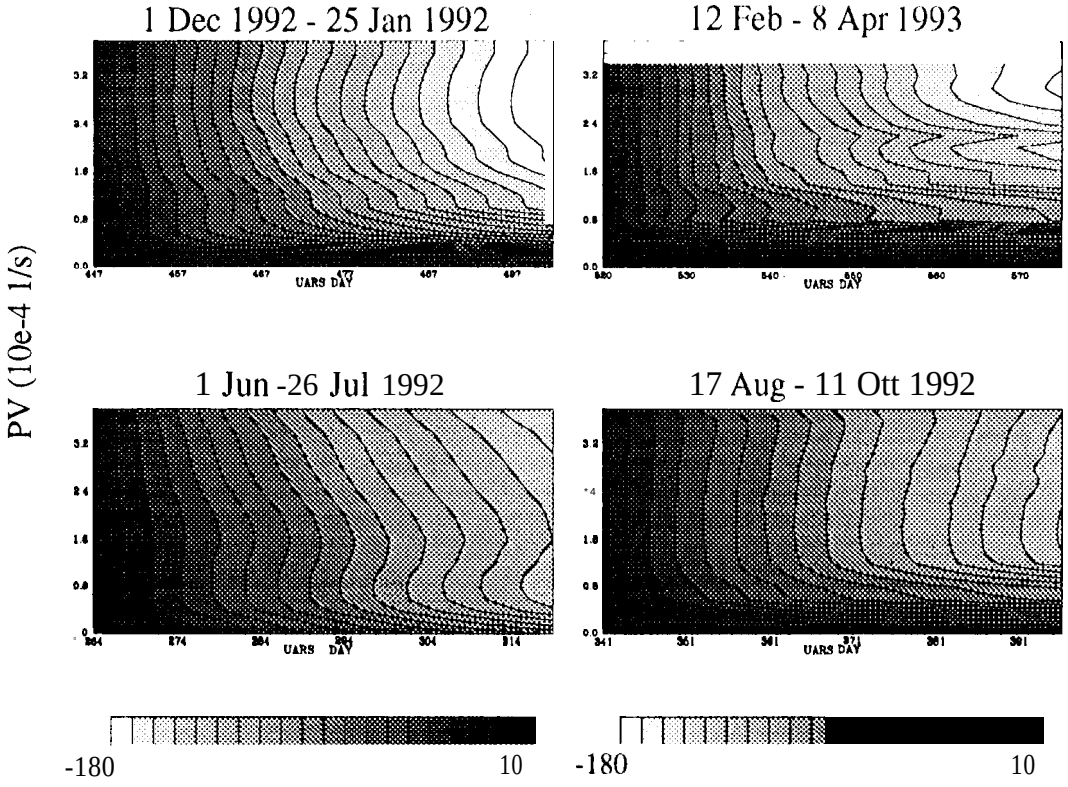
1 Dec 1992 - 25 Jan 1992
12 Feb - 8 Apr 1993
1 Jun -26 Jul 1992
17 Aug - 11 Ott 1992
PV (10e-4 1/s)
UARS DAY
-180
10
-180
10
STARTED 840 K

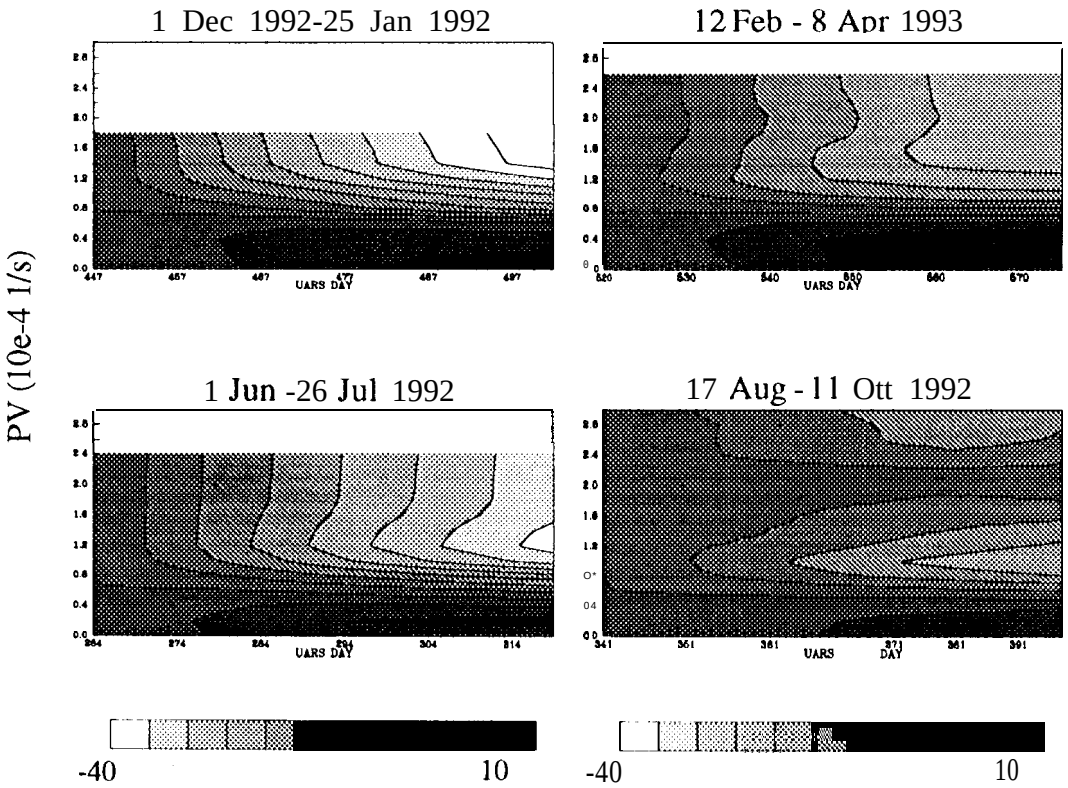
1 Dec 1992-25 Jan 1992
12 Feb - 8 Apr 1993
1 Jun -26 Jul 1992
17 Aug - 11 Ott 1992
PV (10e-4 1/s)
UARS DAY
-40
10
-40
10
STARTED 465 K

Fig. 7

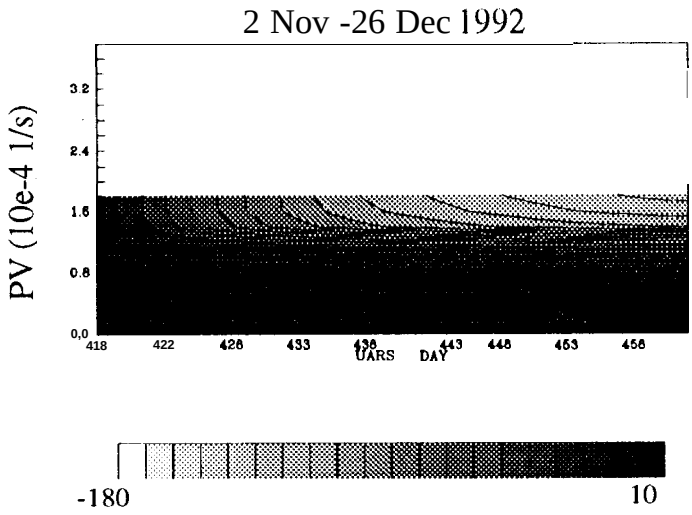
2 Nov -26 Dec 1992
PV (10e-4 1/s)
3.2
2.4
1.6
0.8
0.0
418
422
426
433
436
443
448
453
456
UARS DAY
-180
10
STARTED 840 K

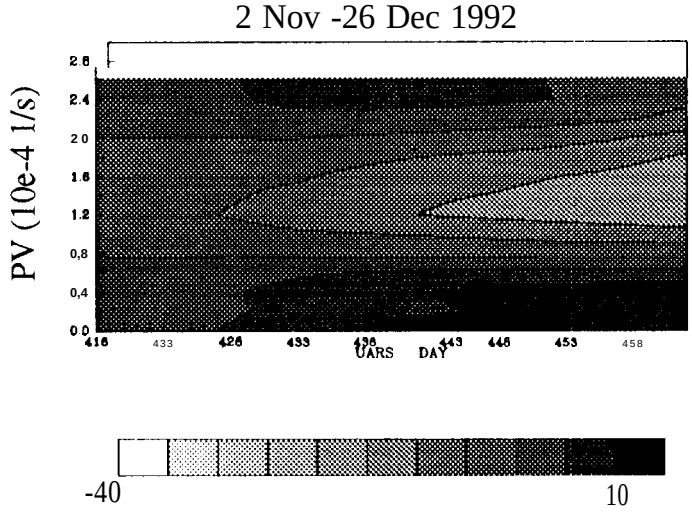
2 Nov -26 Dec 1992
PV (10e-4 1/s)
2.8
2.4
2.0
1.6
1.2
0.8
0.4
0.0
416
433
426
433
436
443
448
453
458
UARS DAY
-40
10
STARTED 465 K

Fig. 7 cont.

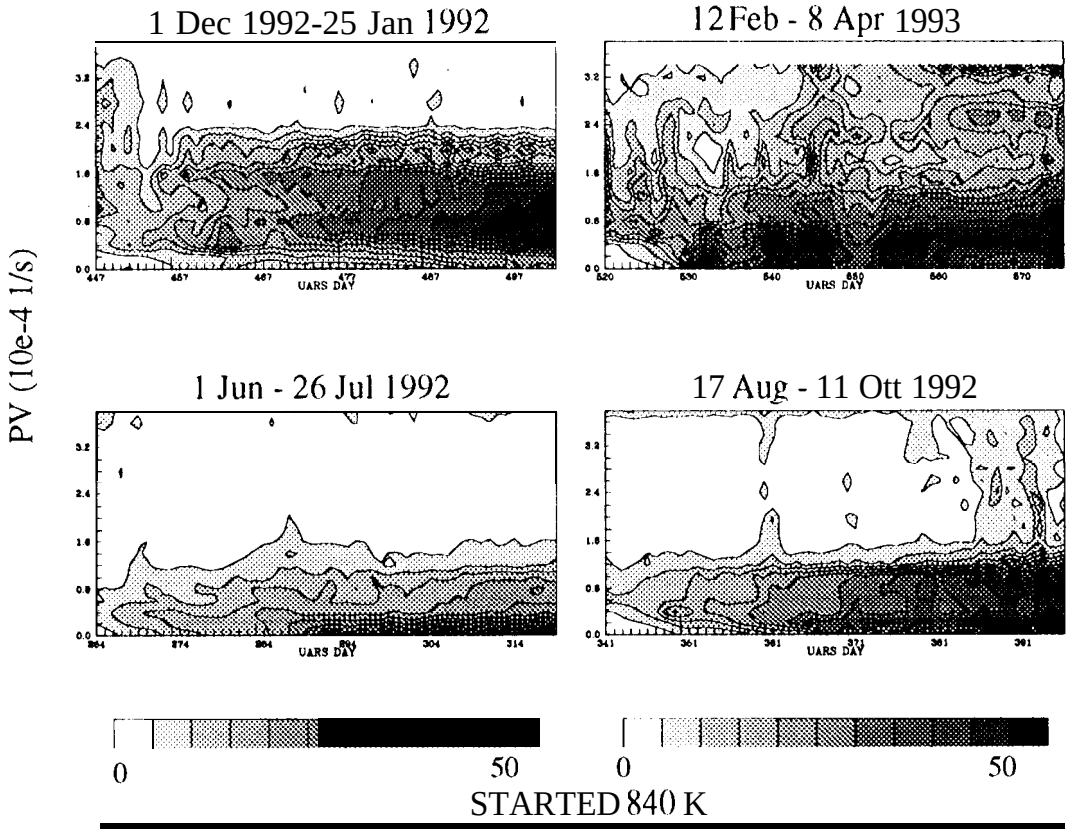
1 Dec 1992-25 Jan 1992
12 Feb - 8 Apr 1993
1 Jun - 26 Jul 1992
17 Aug - 11 Ott 1992
PV (10e-4 1/s)
UARS DAY
0
50
0
50
STARTED 840 K

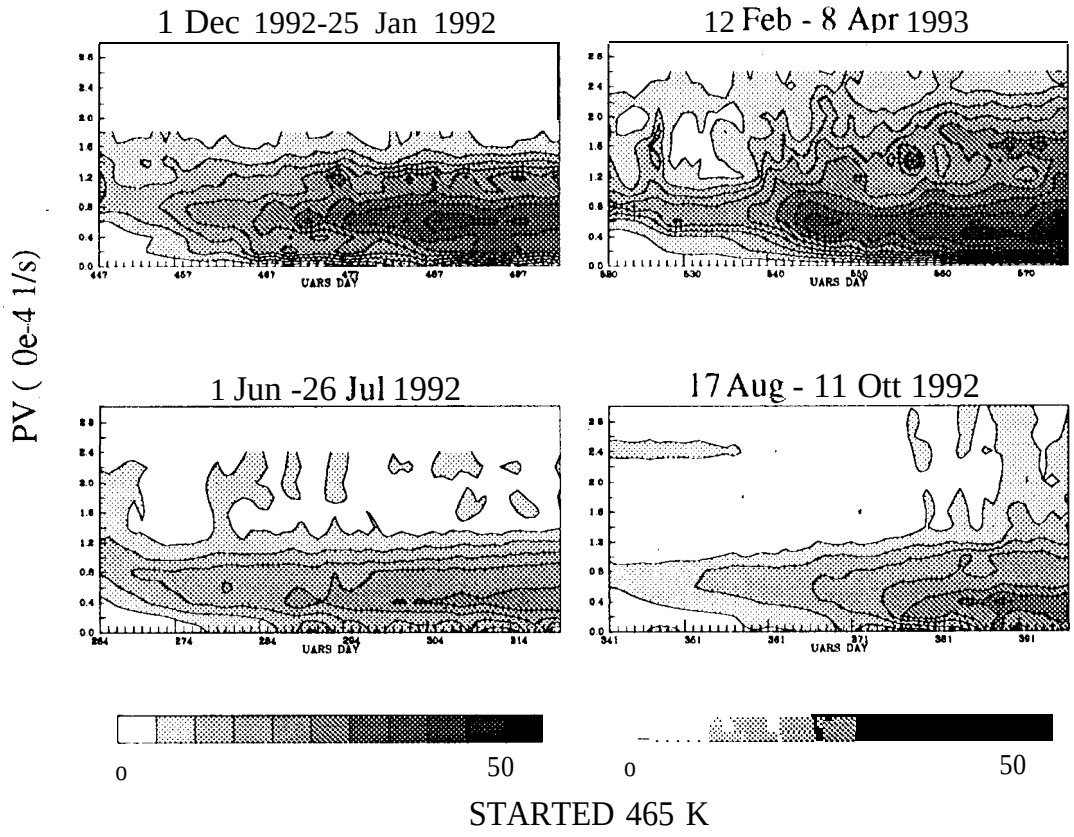
1 Dec 1992-25 Jan 1992
12 Feb - 8 Apr 1993
1 Jun -26 Jul 1992
17 Aug - 11 Ott 1992
PV (0e-4 1/s)
UARS DAY
0
50
0
50
STARTED 465 K

Fig. 8

2 Nov -26 Dec 1992

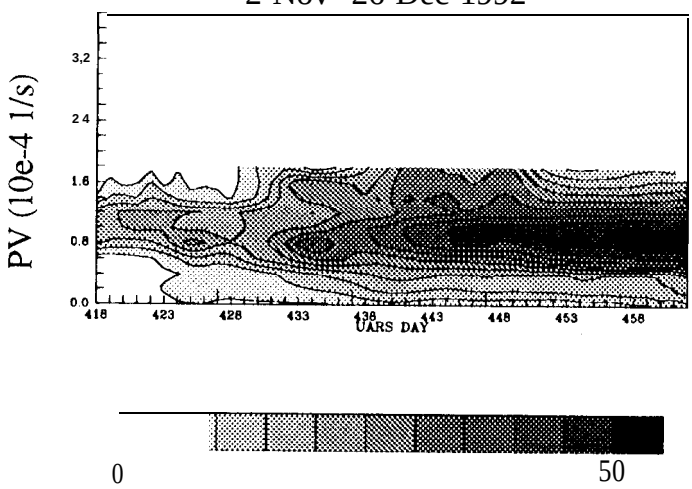

STARTED 840 K

2 Nov -26 Dec 1992

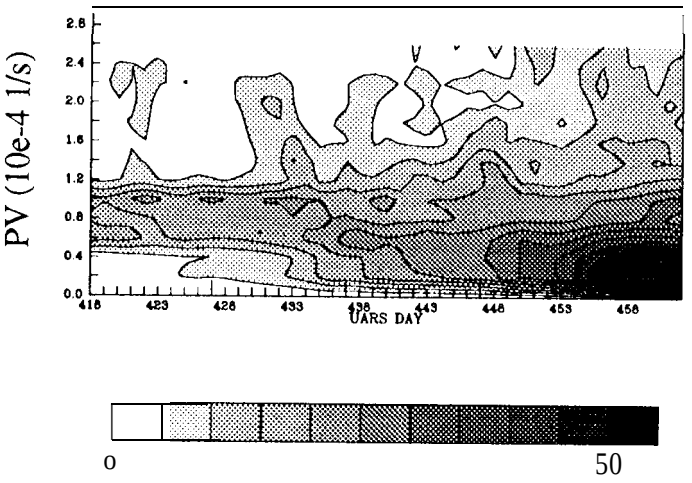

STARTED 465 K

Fig. 8 cont.

1 Dec 992 - 25 Jan 1993

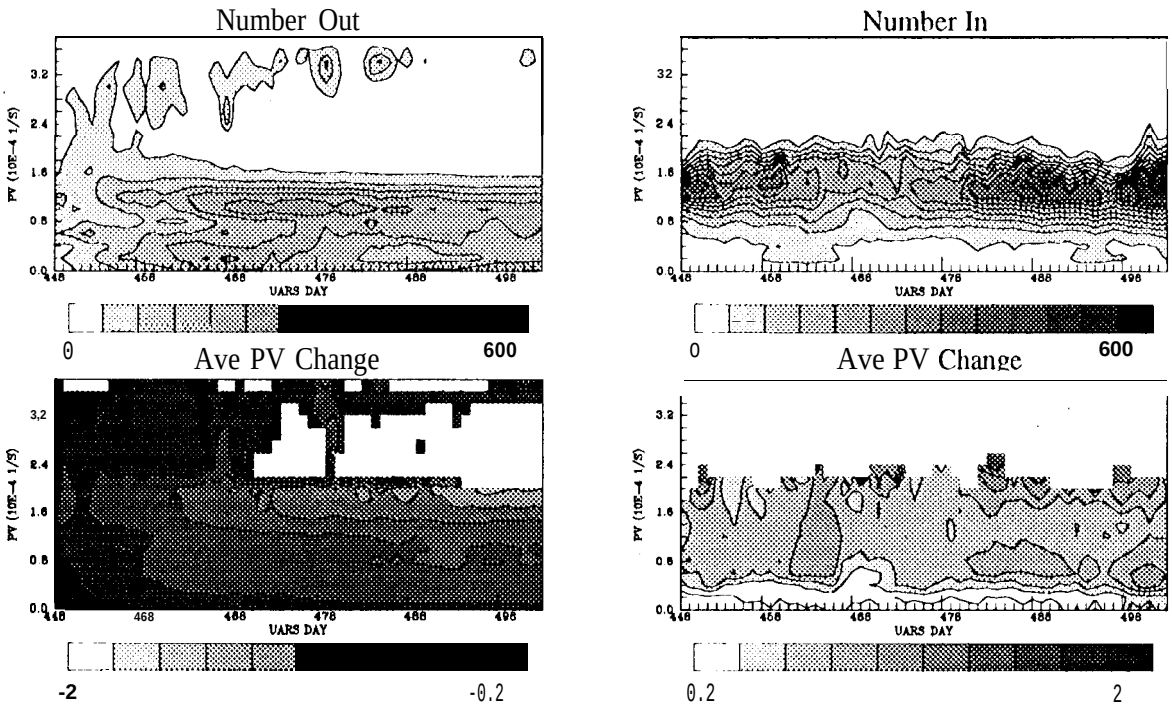

STARTED 840 K

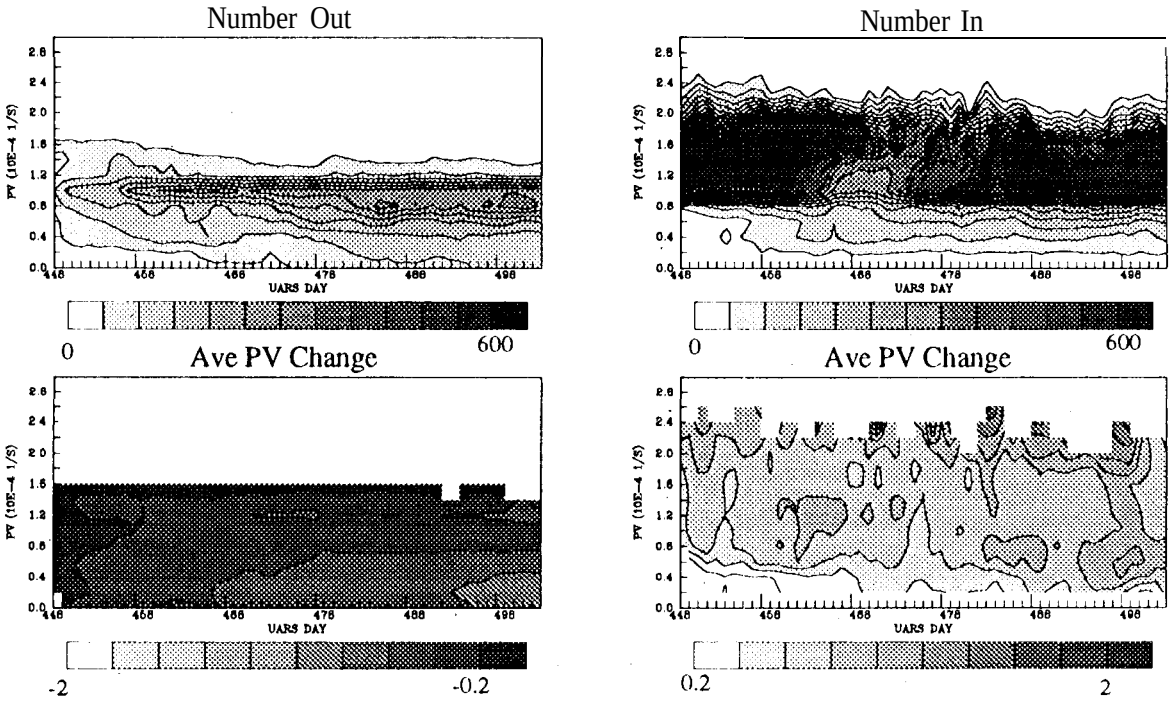

STARTED 465 K

Fig. 9a

12 Feb - 8 Apr 1993

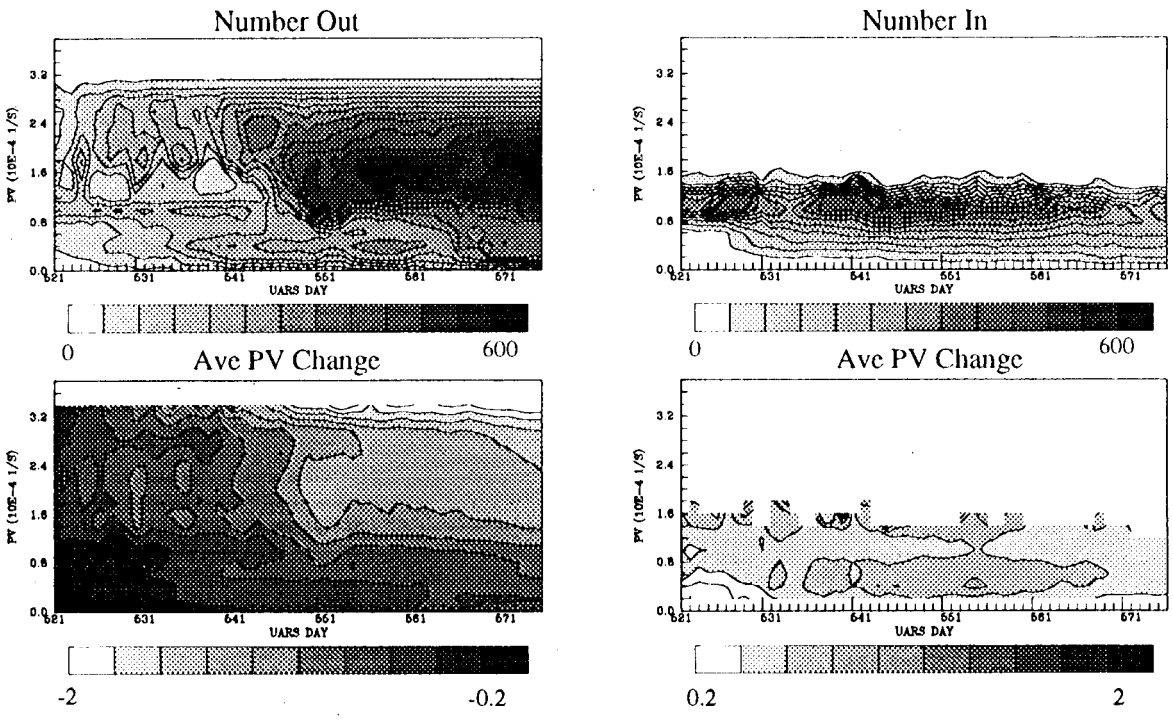

STARTED 840 K

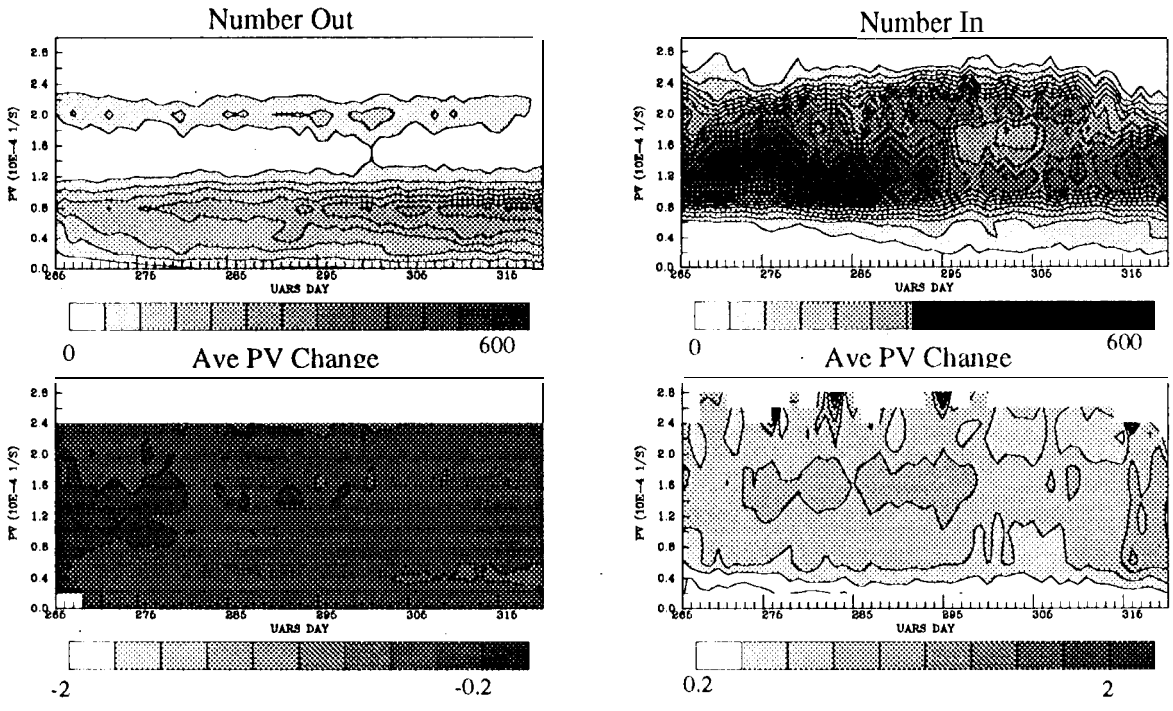

STARTED 465 K

Fig. 9b

1 Jun -26 Jul1992

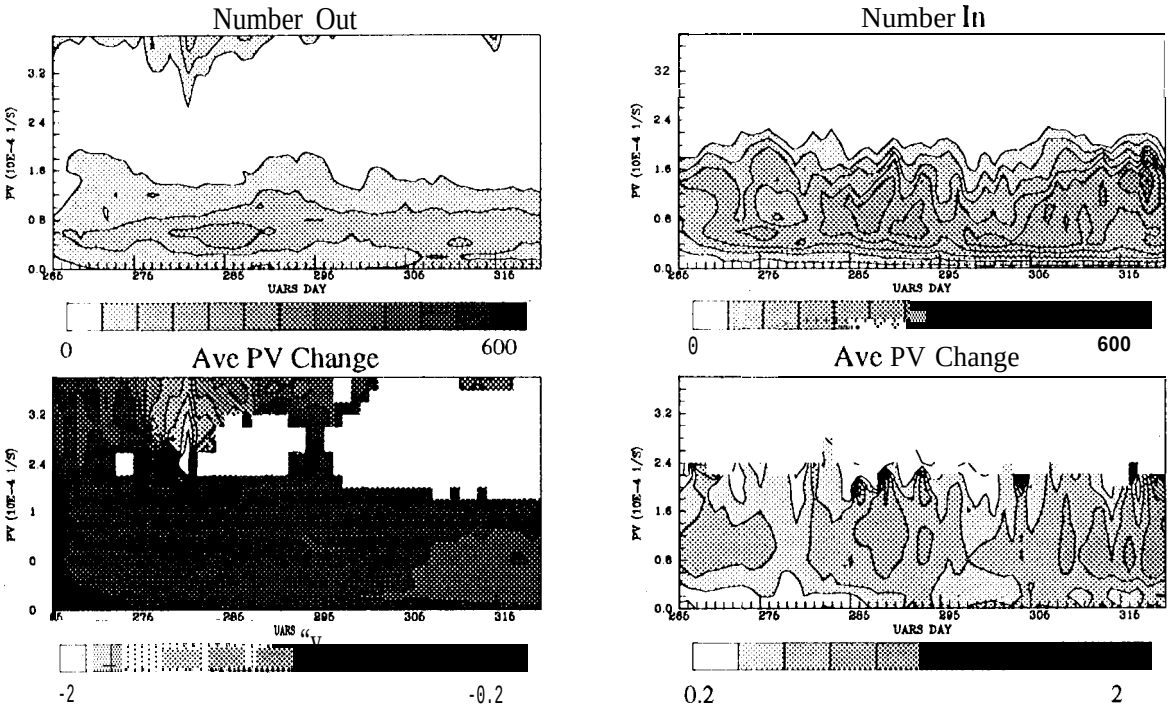

STARTED 840 K

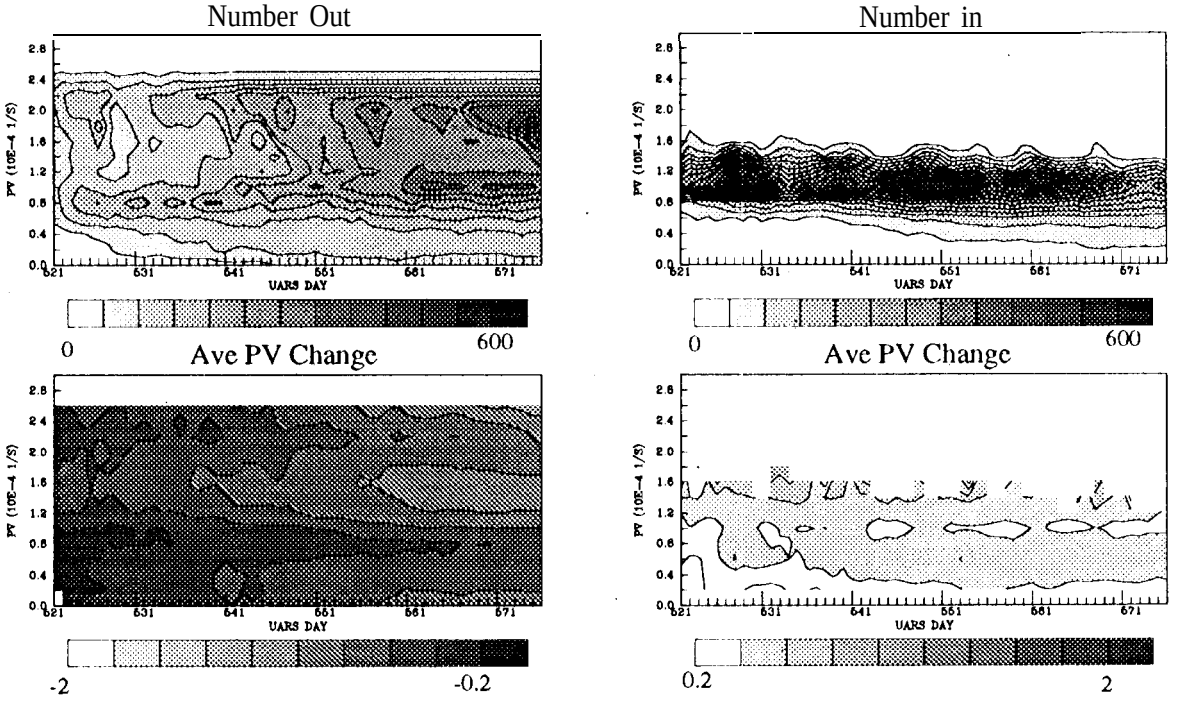

STARTED 465 K

Fig. 9c

17 Aug - 11 Oct 1992

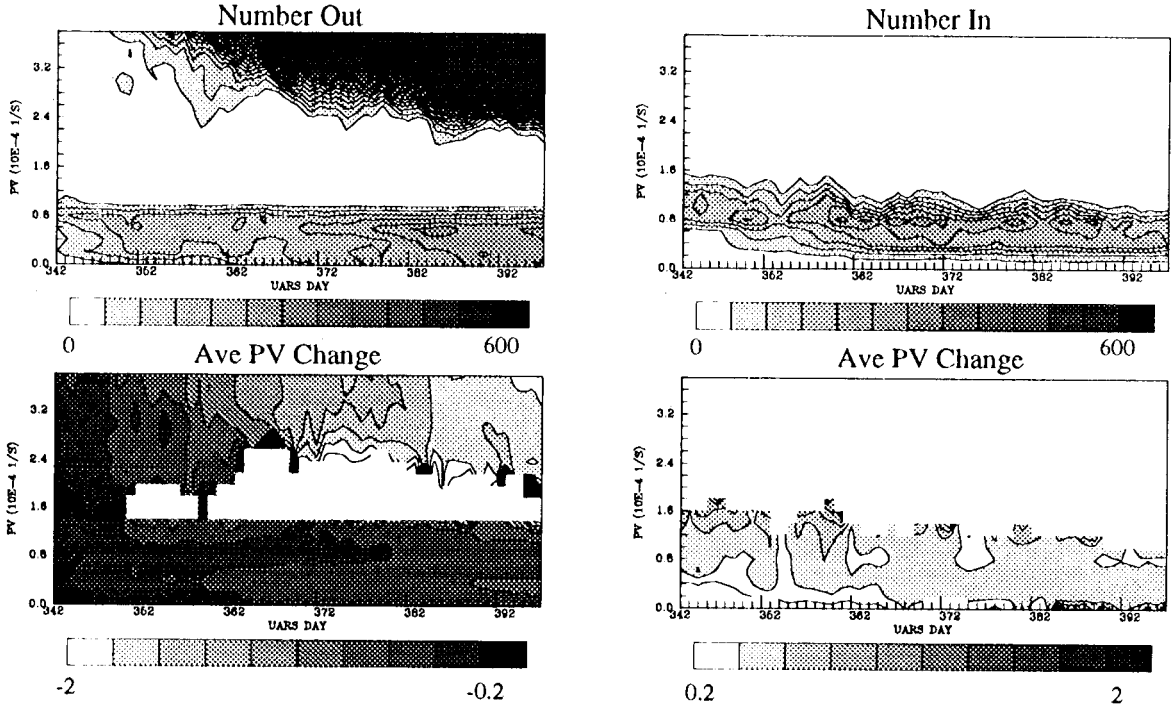

STARTED 840 K

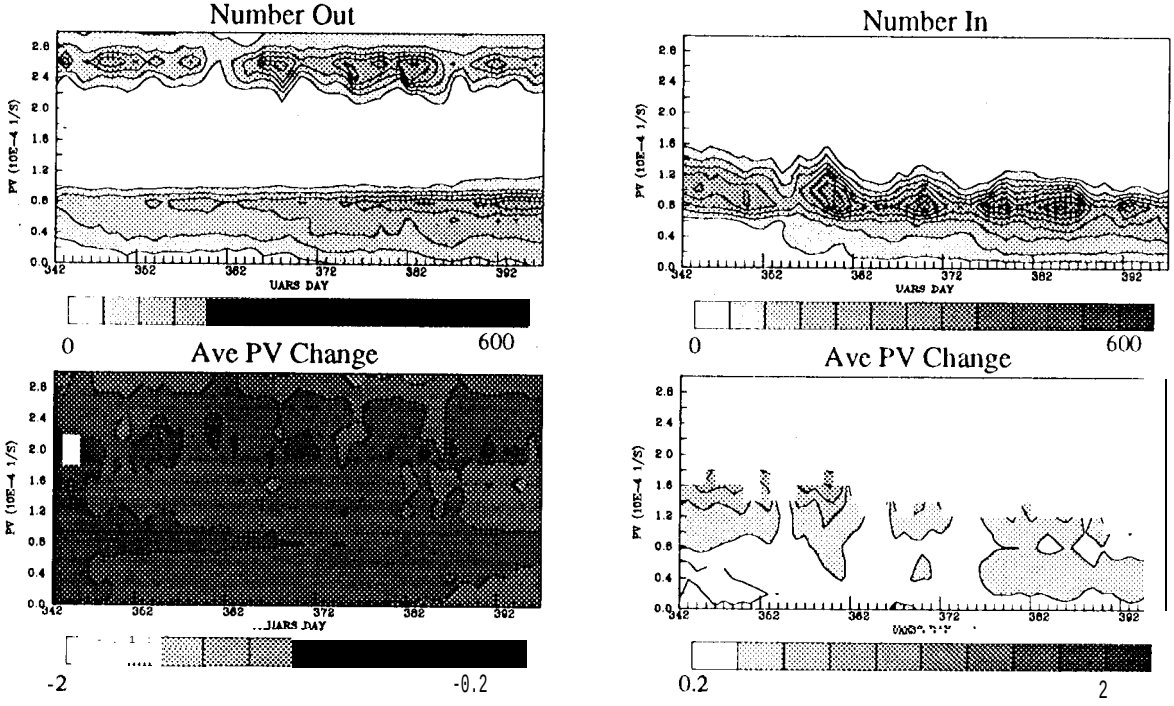

STARTED 465 K

Fig. 9e

2 Nov -26 Dec 1992

Number Out

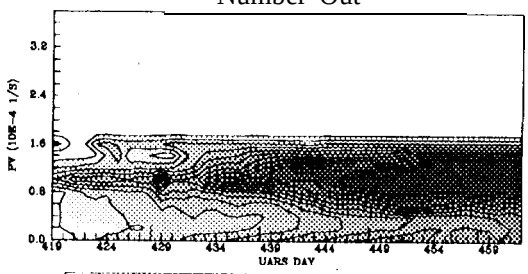

0 600

Ave PV Change

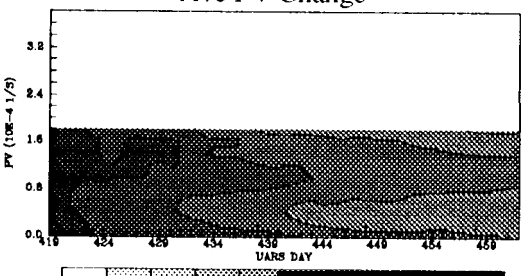

-2 -0.2

STARTED 840 K

Number Out

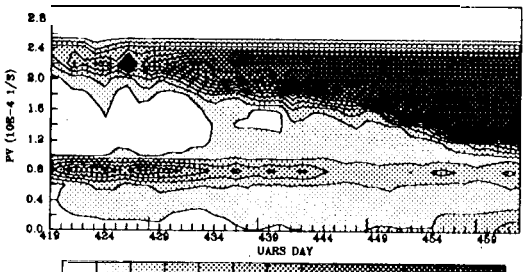

0 600

Ave PV Change

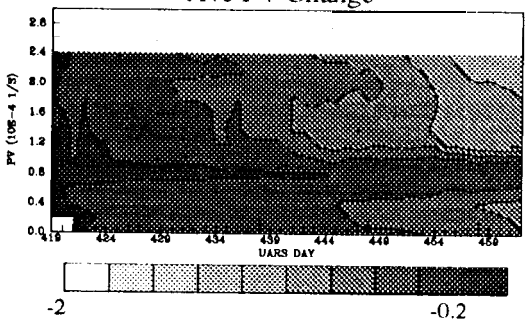

-2 -0.2

STARTED 465 K

Fig. 9f

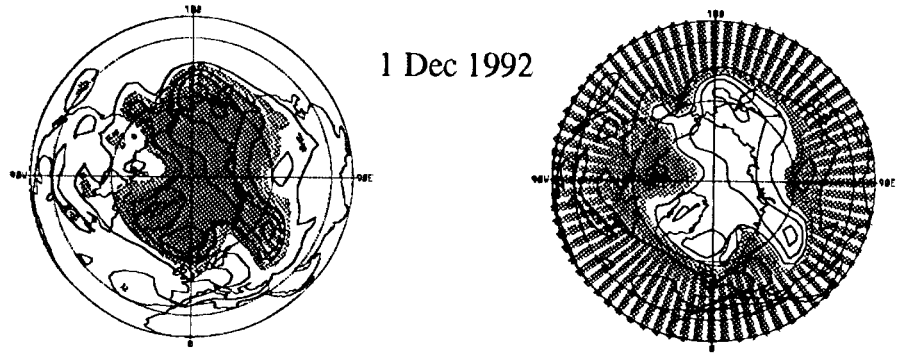

1 Dec 1992

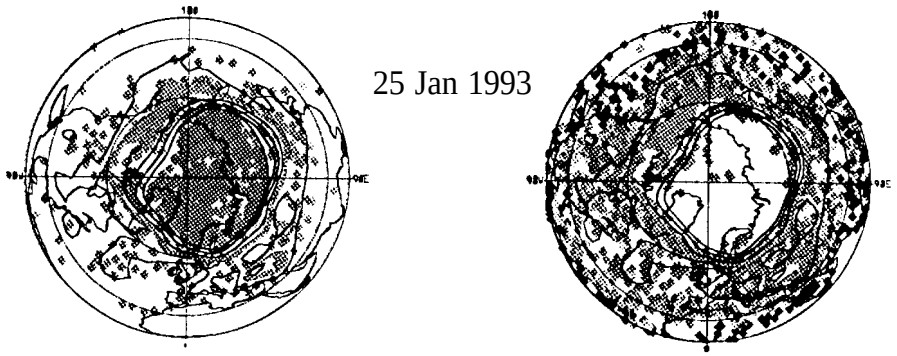

25 Jan 1993

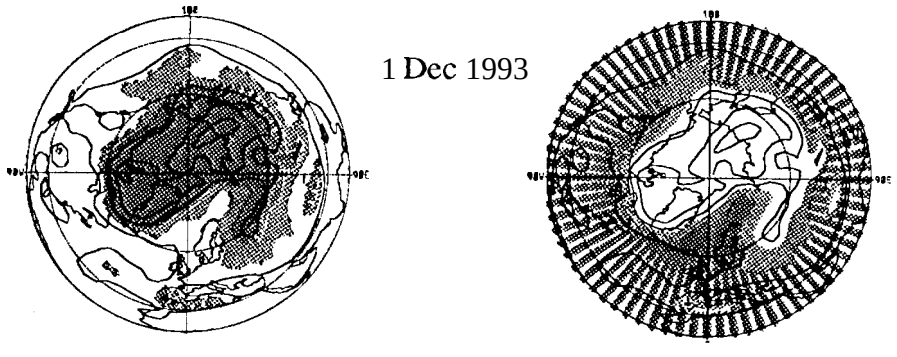

1 Dec 1993

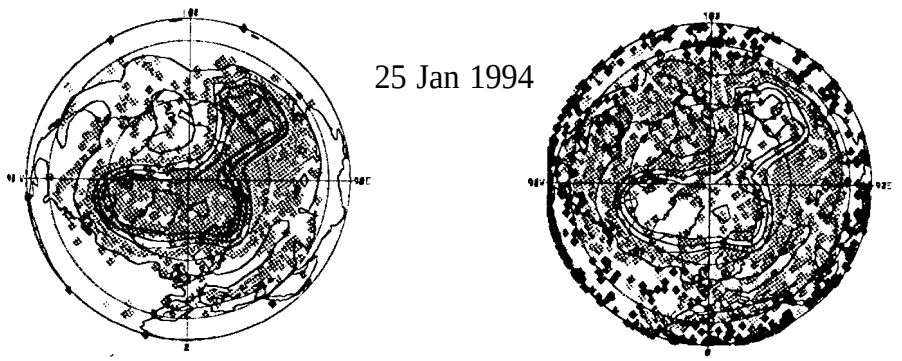

25 Jan 1994

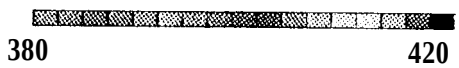

380 420

380 420

Fig. 10 a, b

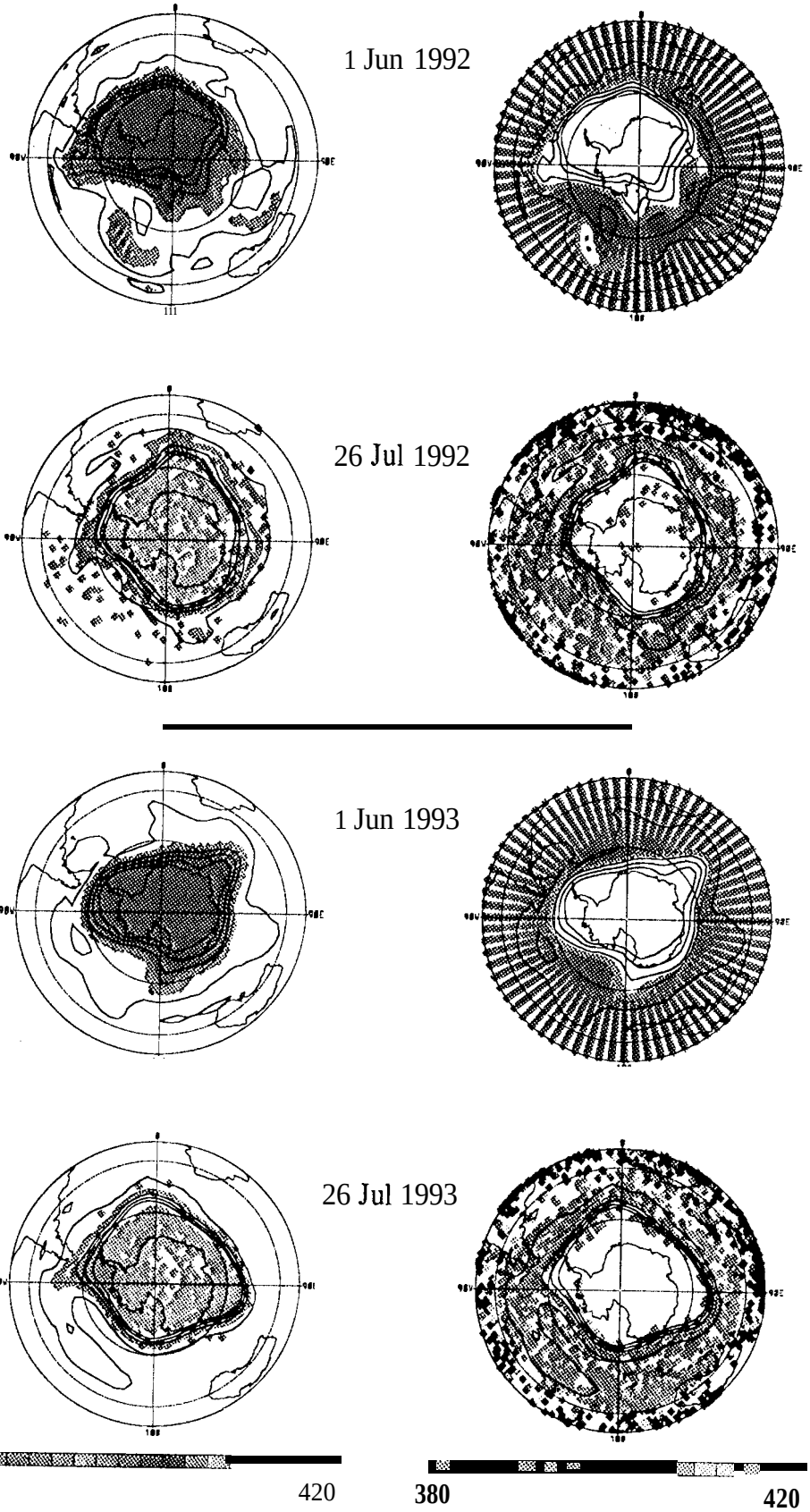

Fig. 10c, d

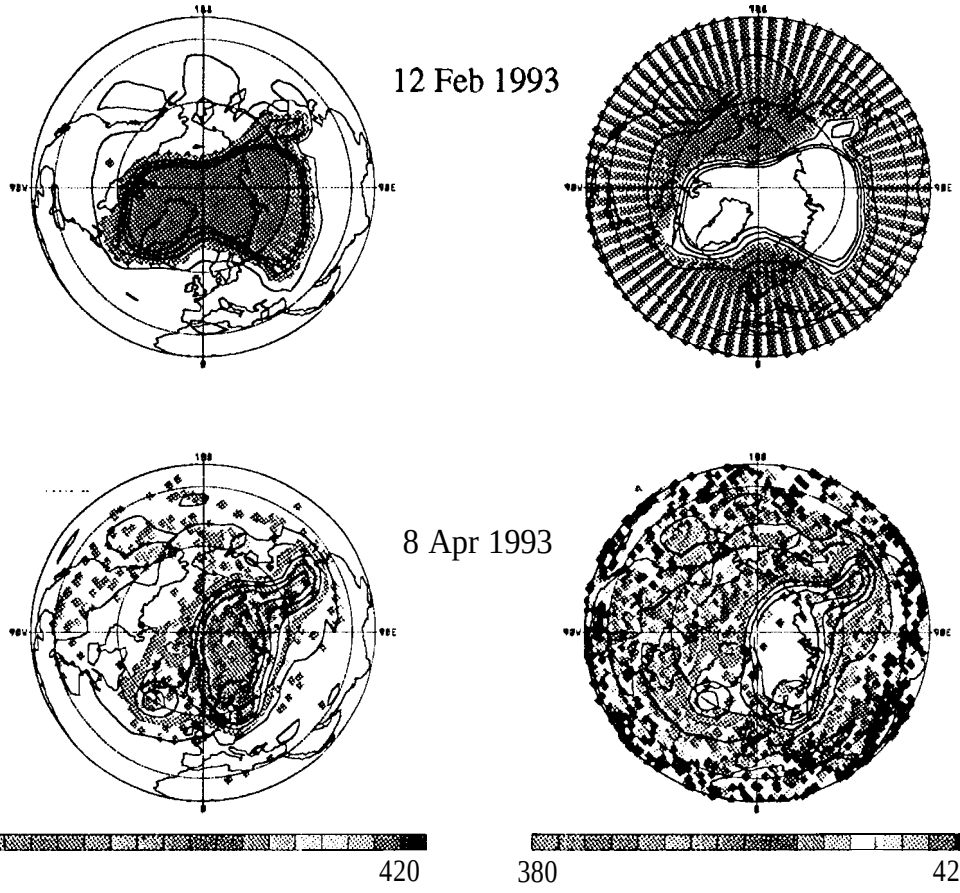

Fig. 10e

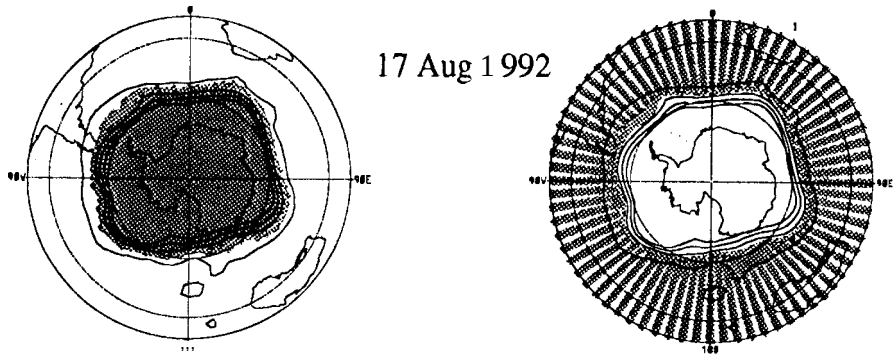

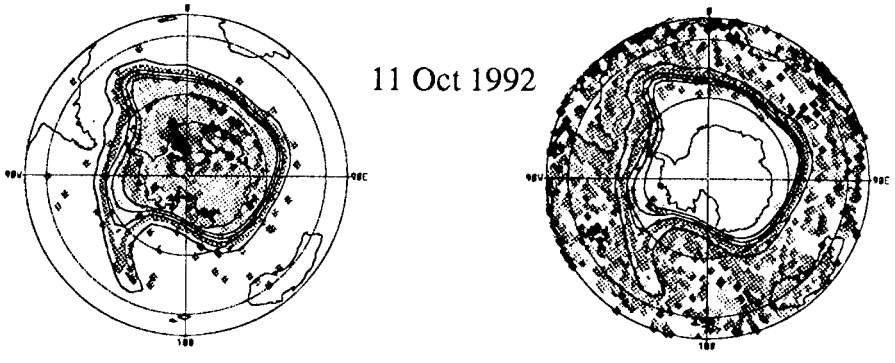

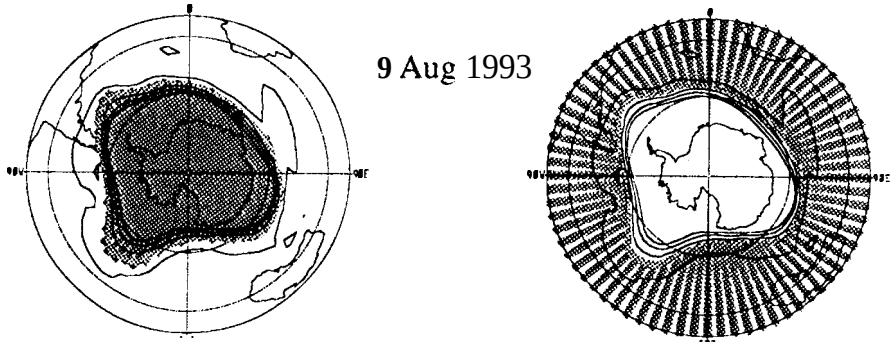

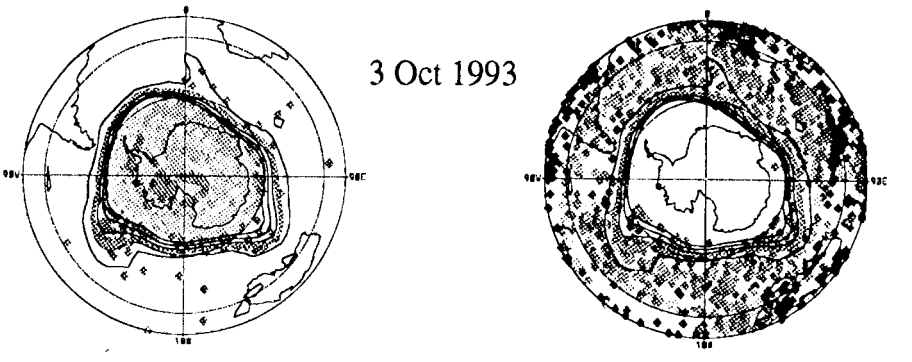

Fig. 10 f, g

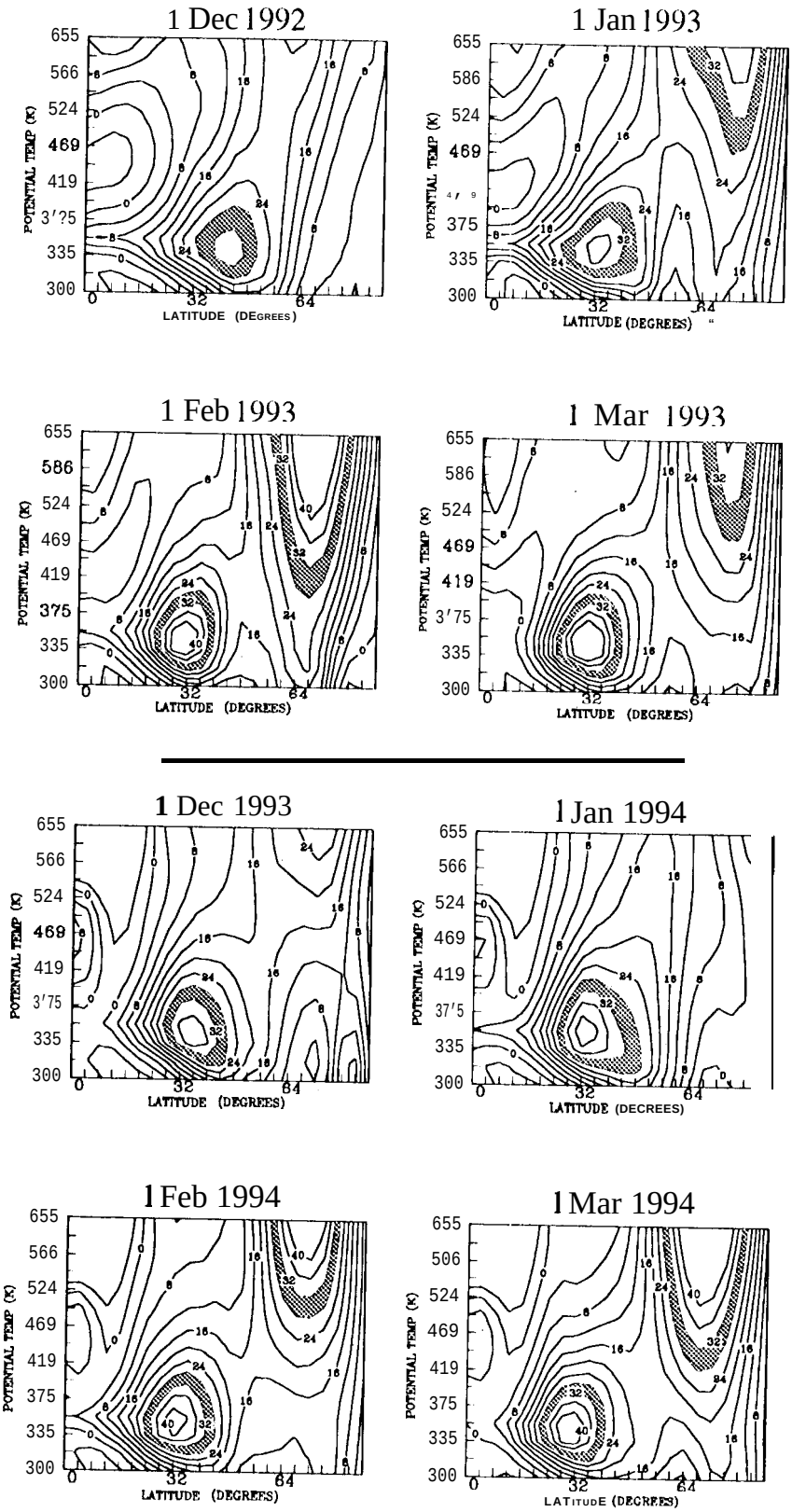
1 Dec 1992
1 Jan 1993
1 Feb 1993
1 Mar 1993
1 Dec 1993
1 Jan 1994
1 Feb 1994
1 Mar 1994
POTENTIAL TEMP (K)
LATITUDE (DEGREES)
655
586
566
524
469
419
375
335
300
0
32
64

Fig. 11

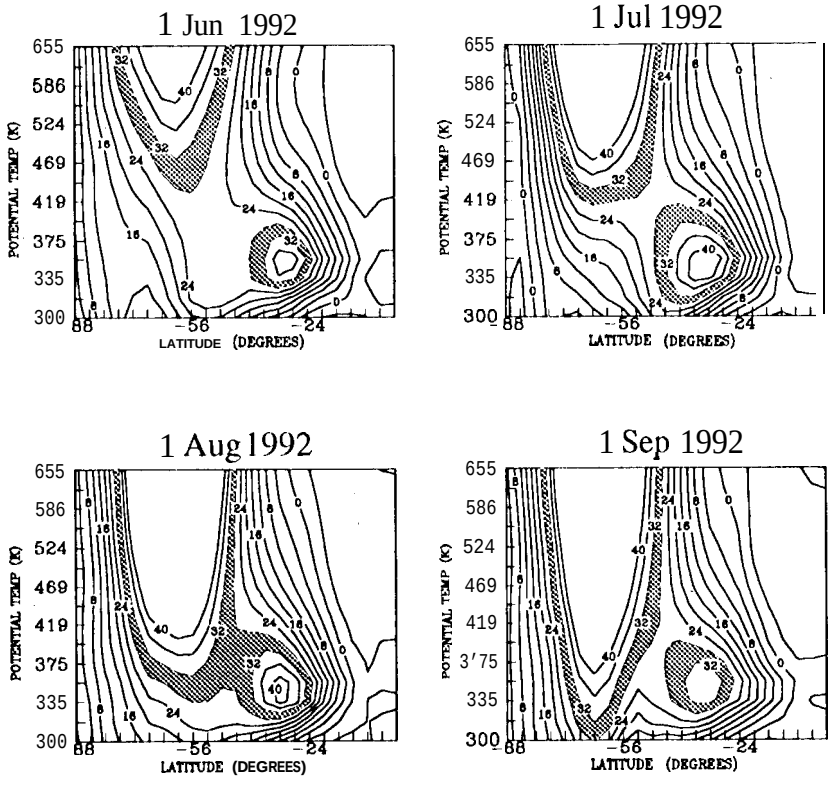
1 Jun 1992
1 Jul 1992
1 Aug 1992
1 Sep 1992
1 Jun 1993
1 Jul 1993
1 Aug 1993
1 Sep 1993
POTENTIAL TEMP (K)
LATITUDE (DEGREES)
655
586
524
469
419
375
335
300
-88
-56
-24

Fig. 11 cont.

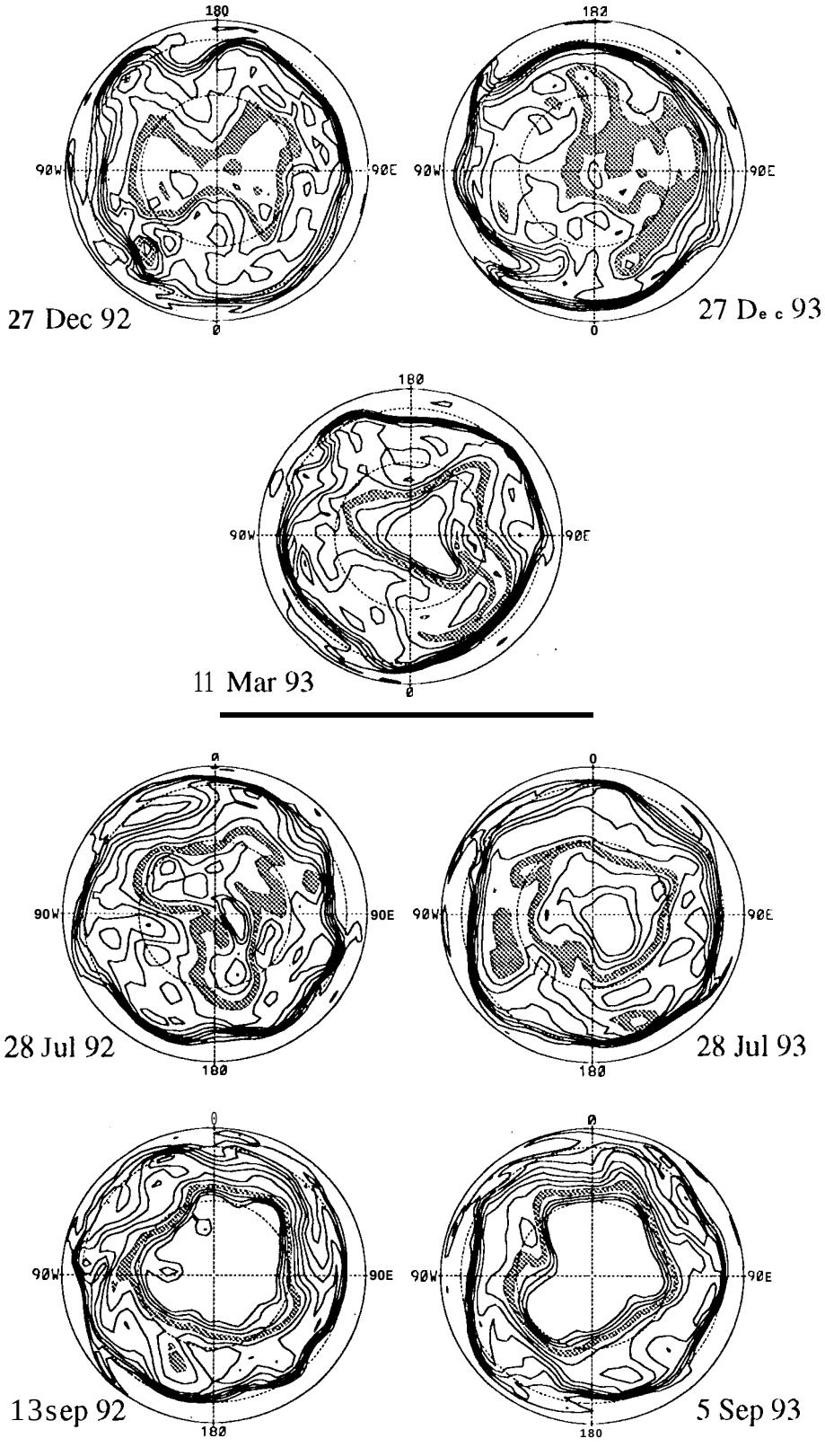
180
90W
90E
0
27 Dec 92
27 Dec 93
11 Mar 93
28 Jul 92
28 Jul 93
13sep 92
5 Sep 93

Fig. 12

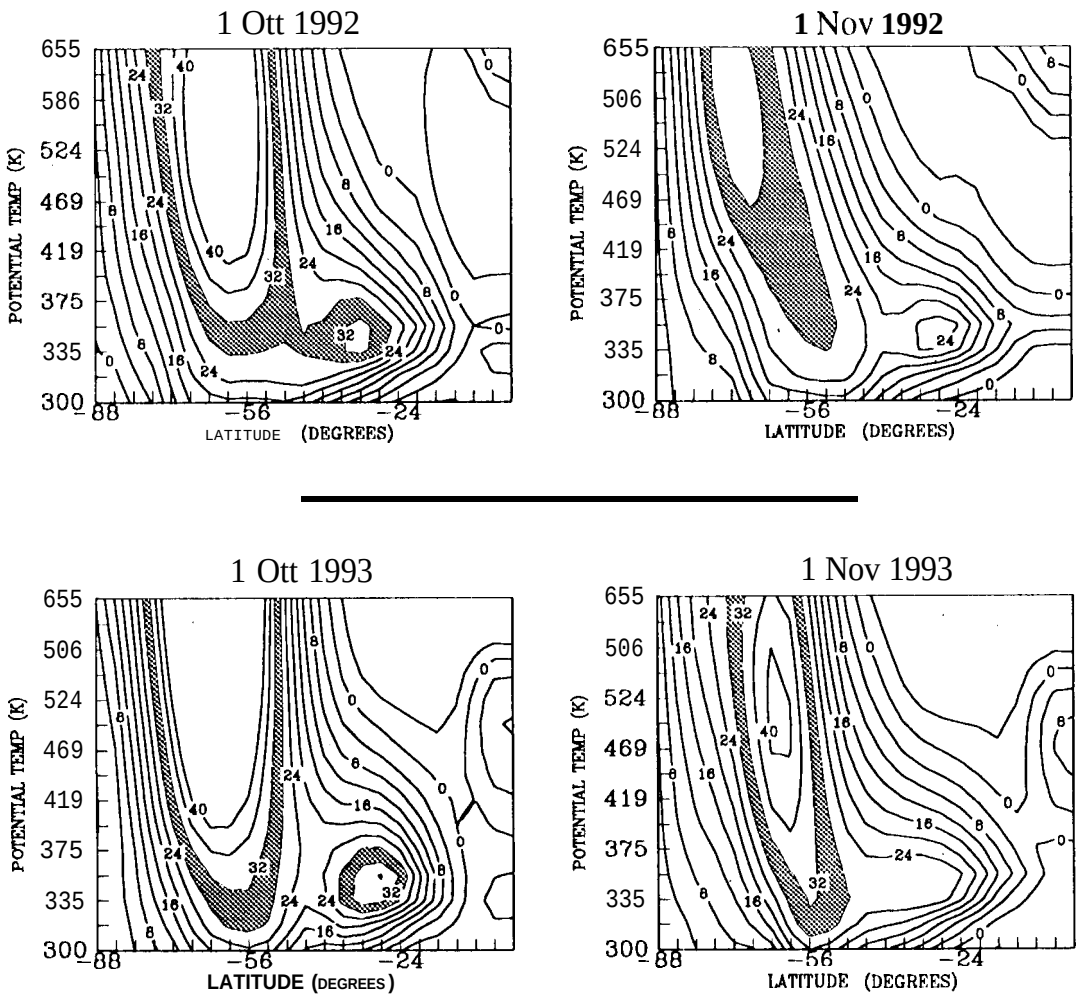
1 Ott 1992
1 Nov 1992
1 Ott 1993
1 Nov 1993
POTENTIAL TEMP (K)
655
586
524
469
419
375
335
300
-88
-56
-24
LATITUDE (DEGREES)

Fig. 13

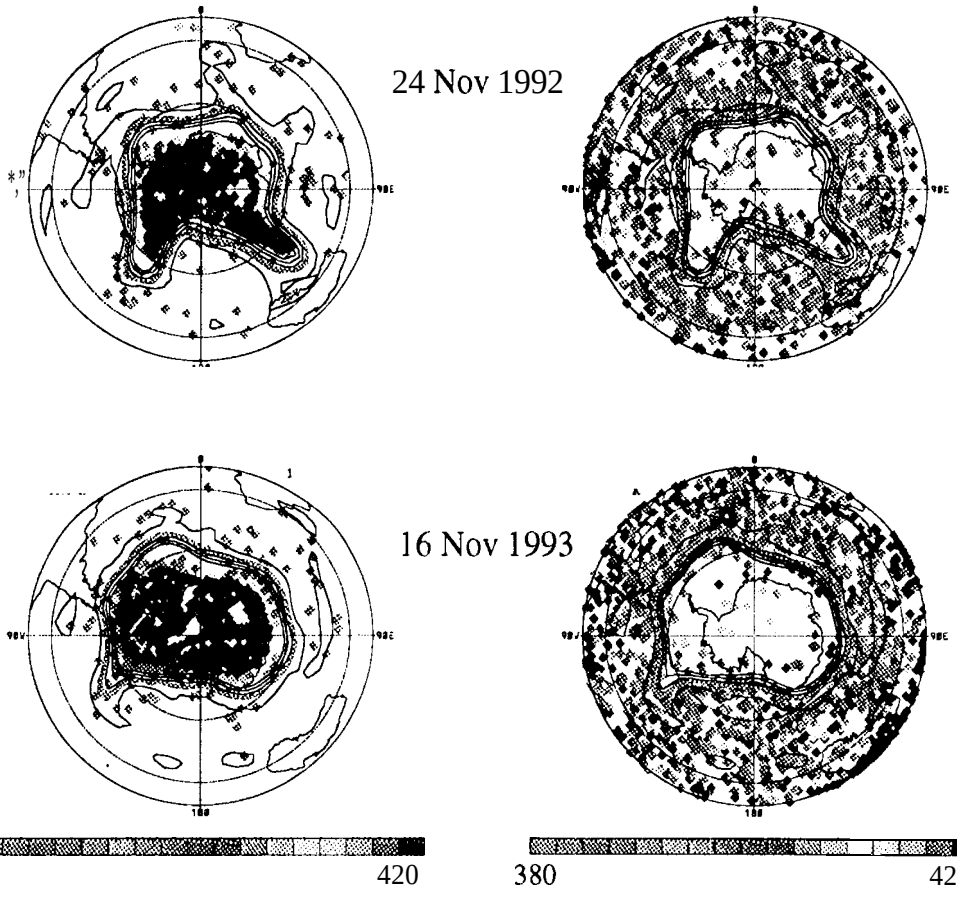

Fig. 14

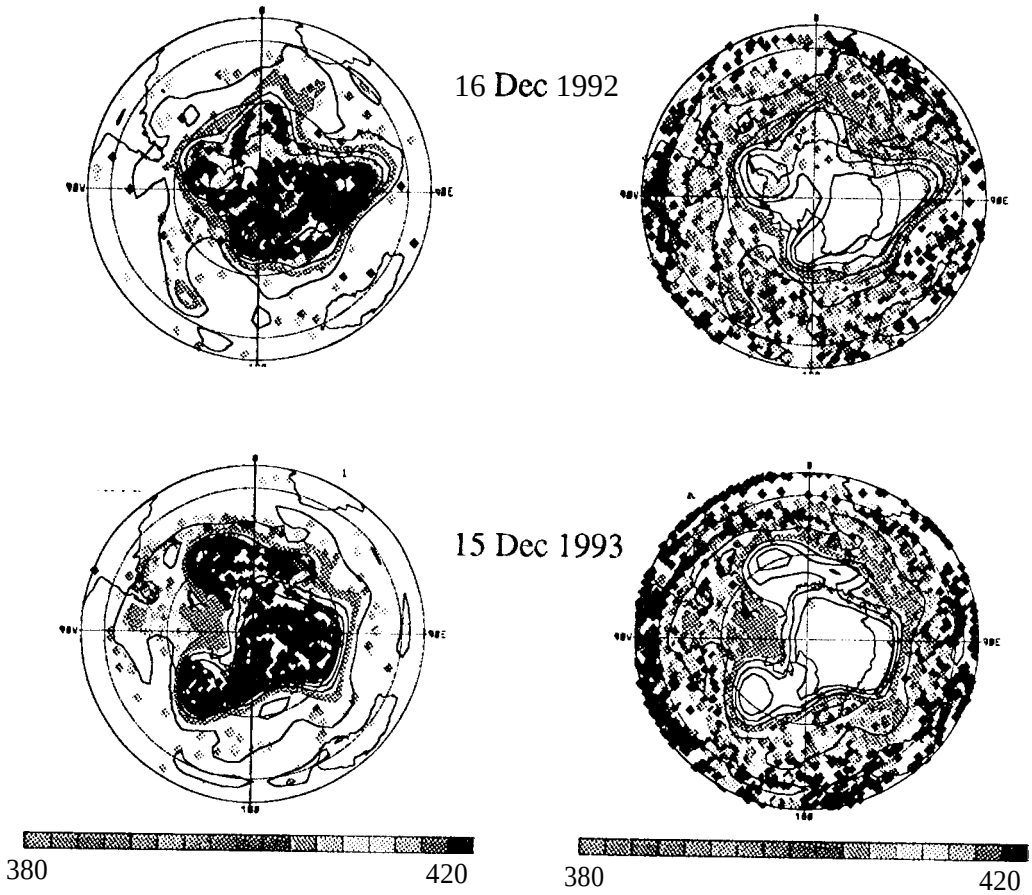

Fig. 15

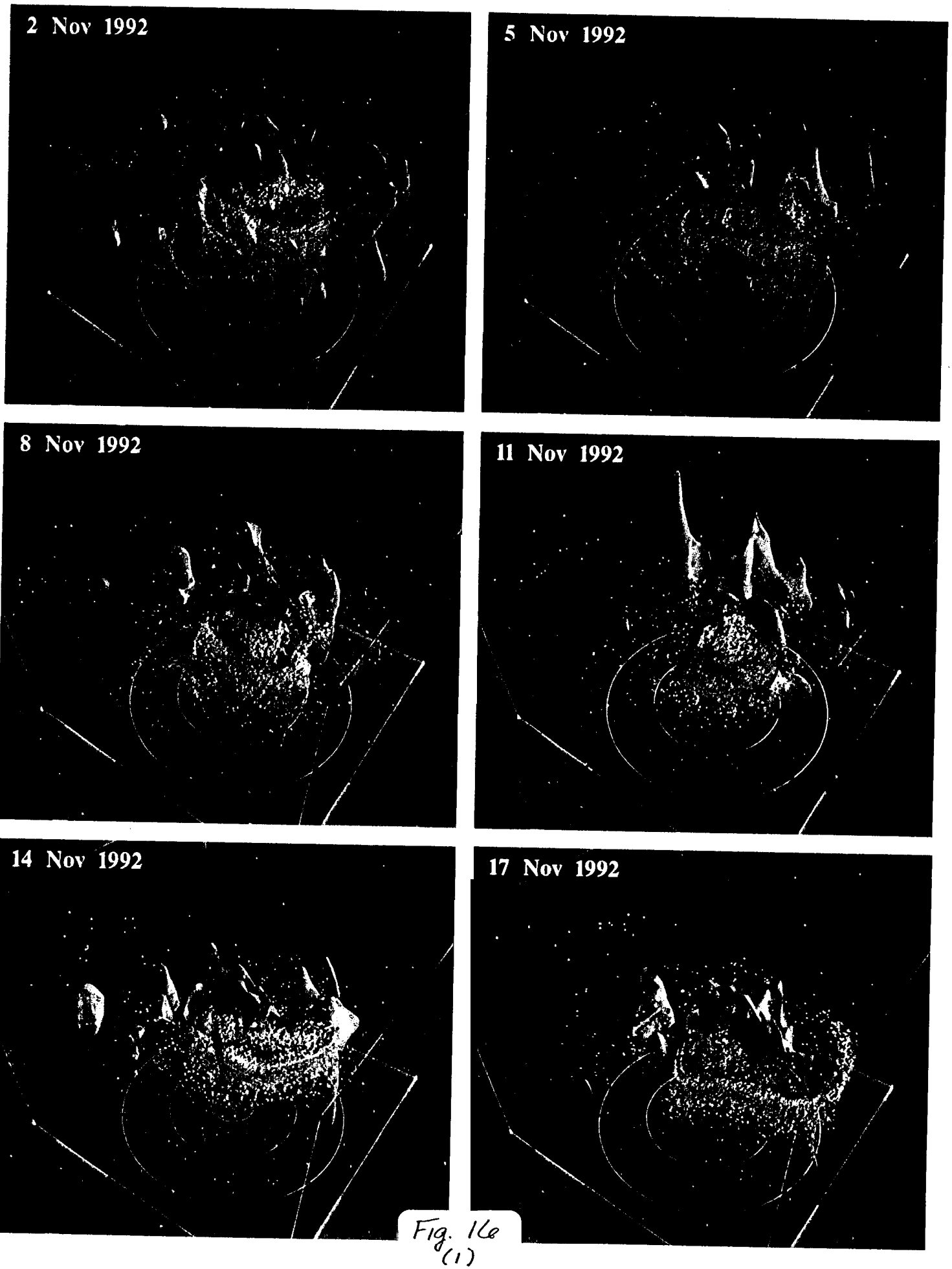
2 Nov 1992
5 Nov 1992
8 Nov 1992
11 Nov 1992
14 Nov 1992
17 Nov 1992

Fig. 16
(1)


20 Nov 1992


23 Nov 1992


26 Nov 1992


29 Nov 1992


2 Dec 1992

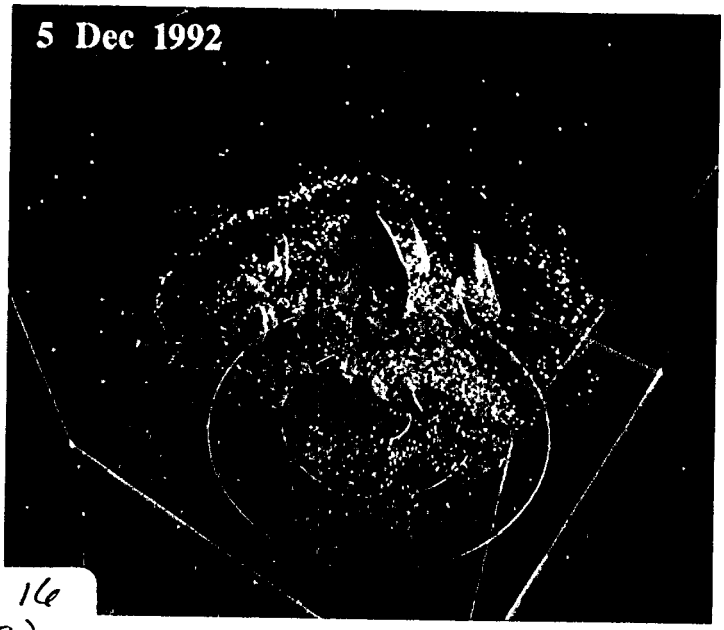
5 Dec 1992

Fig 16
(2)

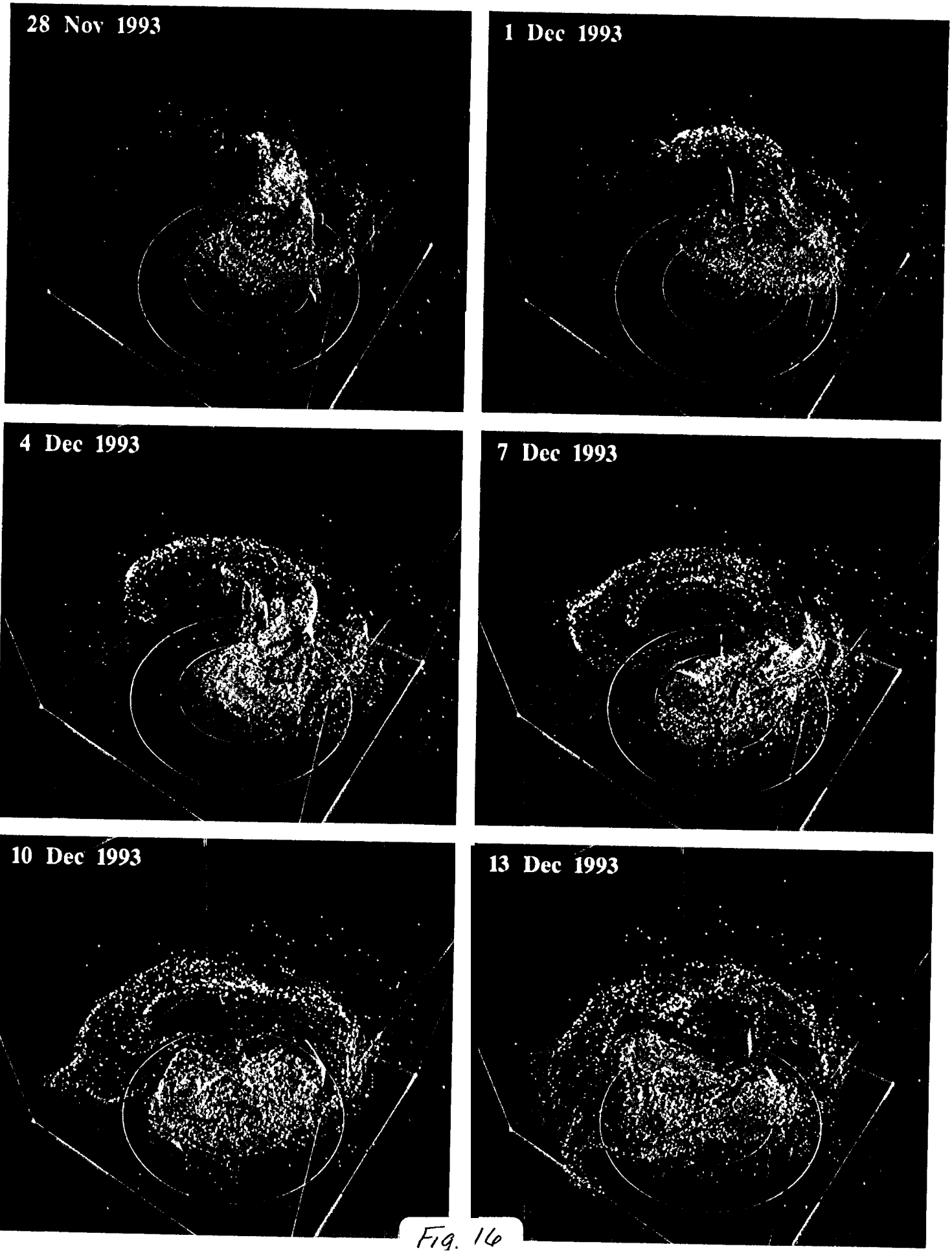
28 Nov 1993
1 Dec 1993
4 Dec 1993
7 Dec 1993
10 Dec 1993
13 Dec 1993

Fig. 16

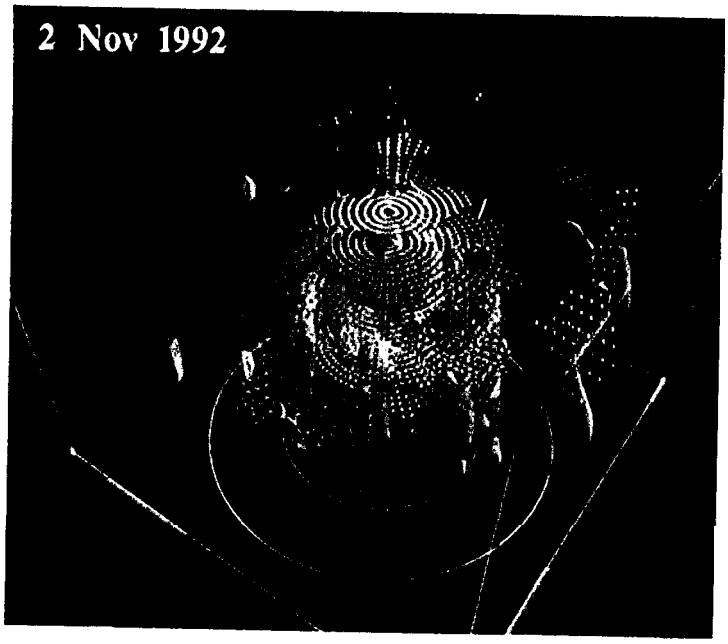
2 Nov 1992

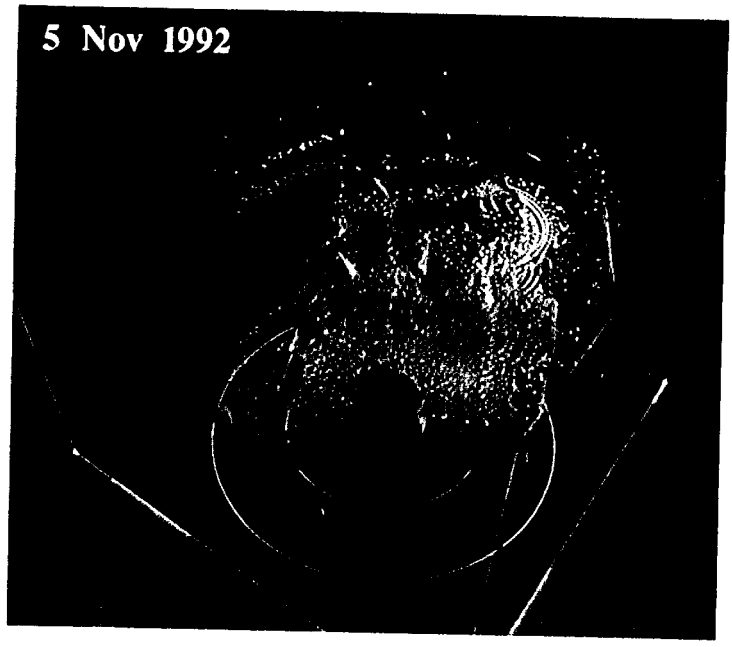
5 Nov 1992

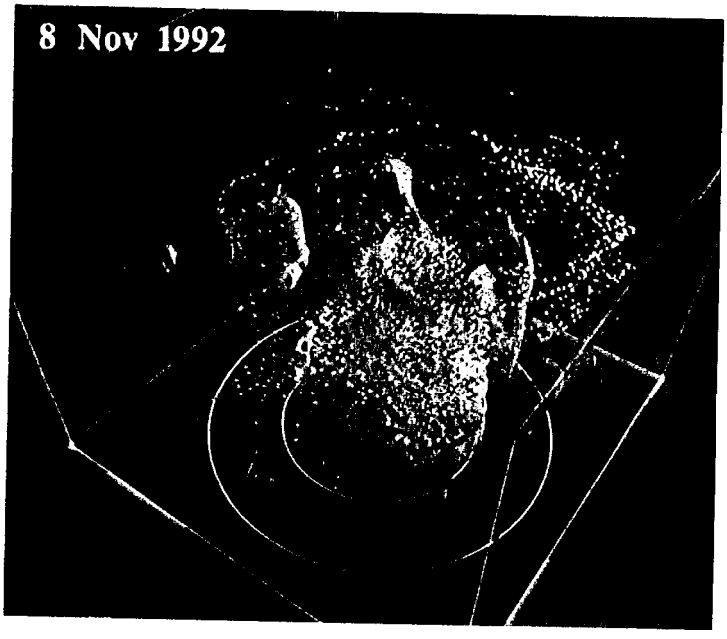
8 Nov 1992

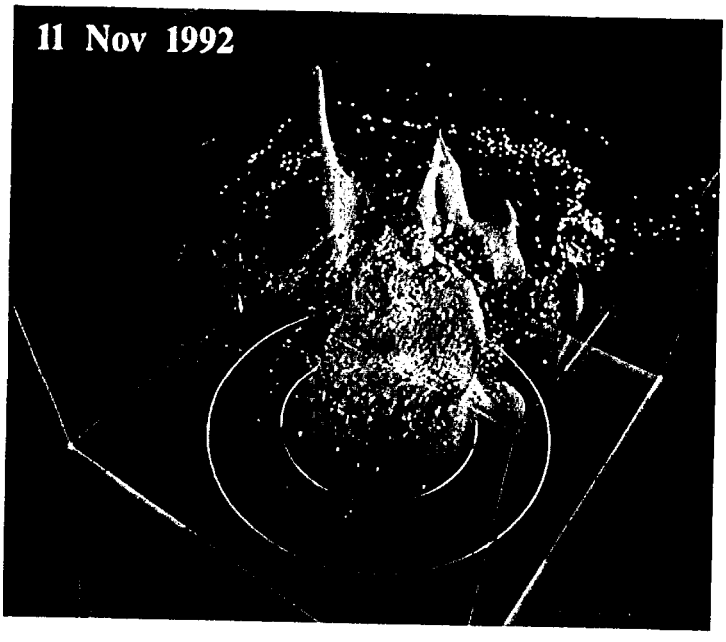
11 Nov 1992

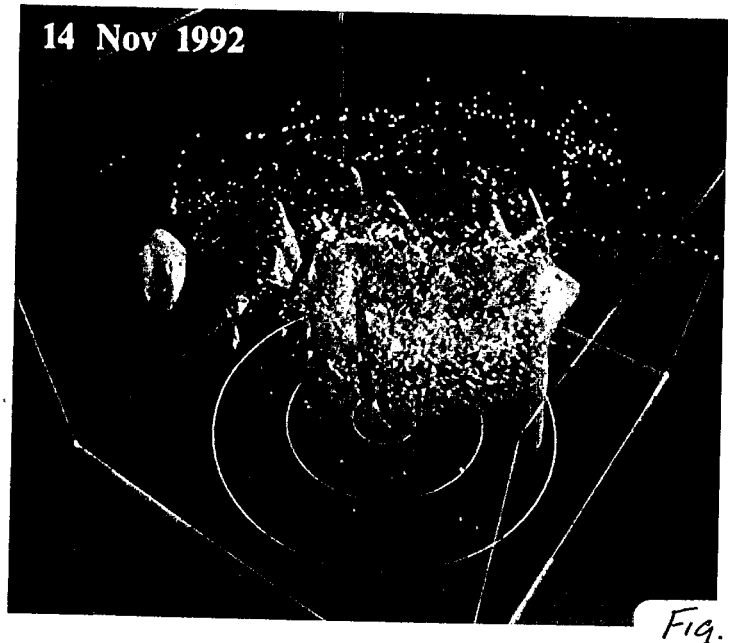
14 Nov 1992

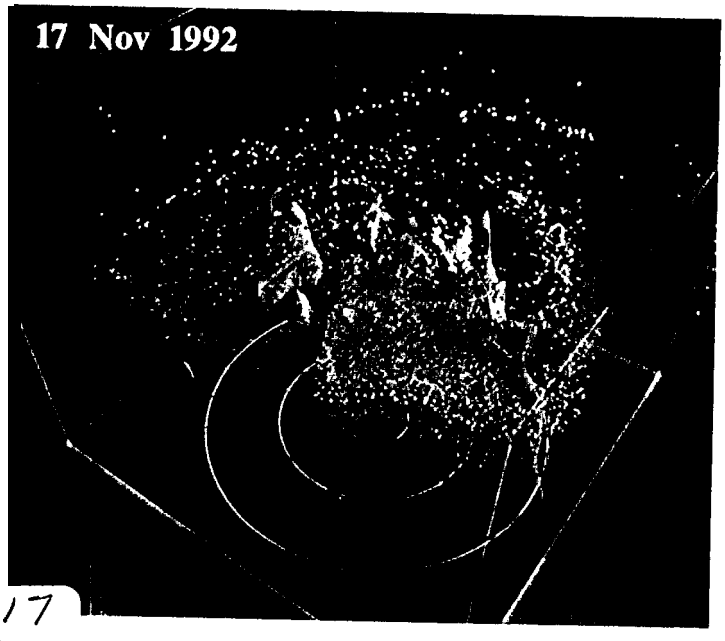
17 Nov 1992

Fig. 17
(1)

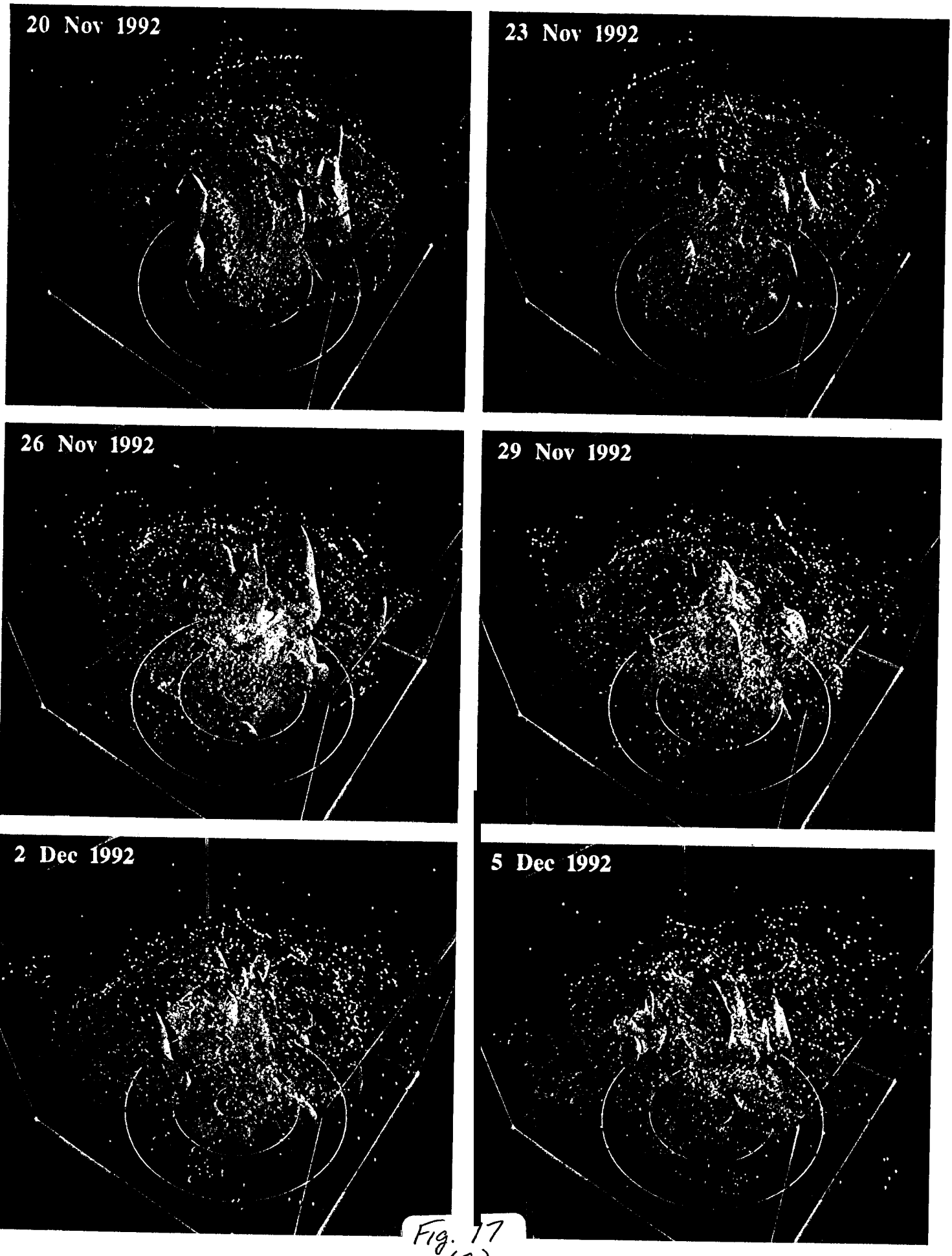
20 Nov 1992
23 Nov 1992
26 Nov 1992
29 Nov 1992
2 Dec 1992
5 Dec 1992

Fig. 17
(2)

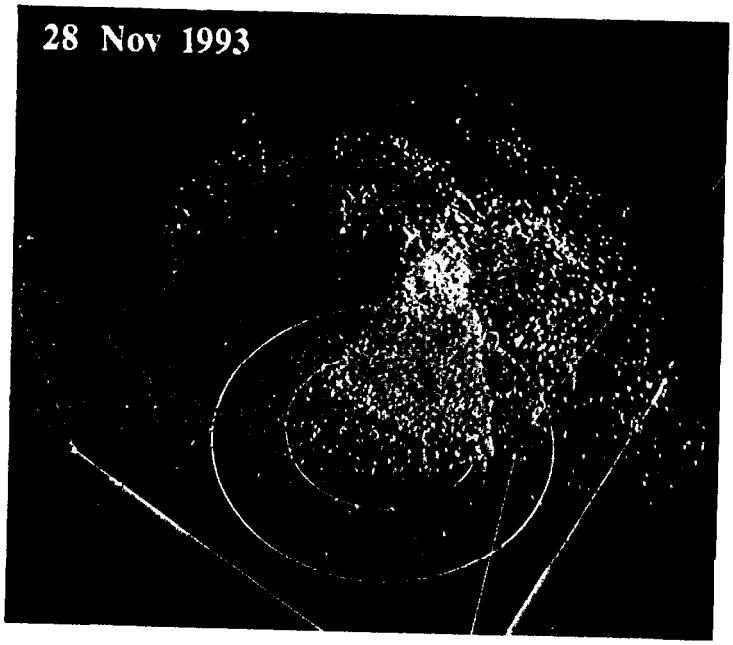
28 Nov 1993

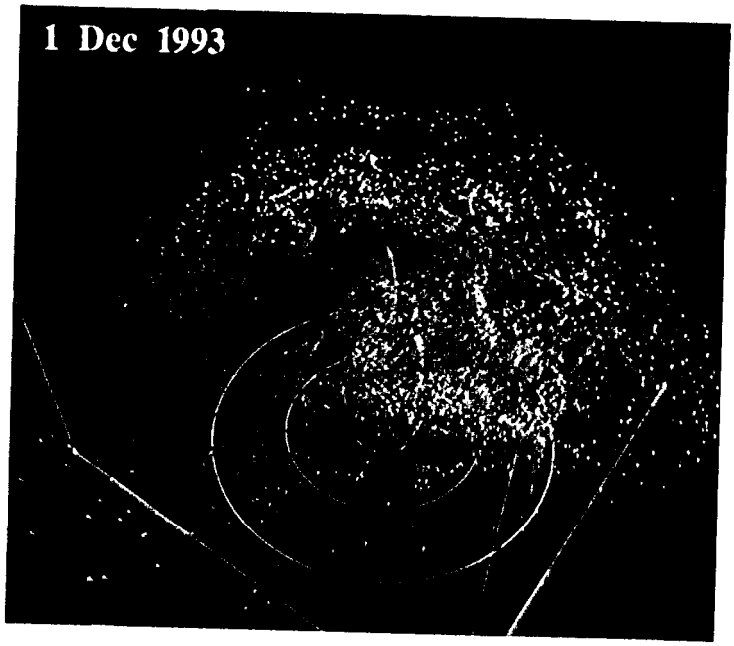
1 Dec 1993

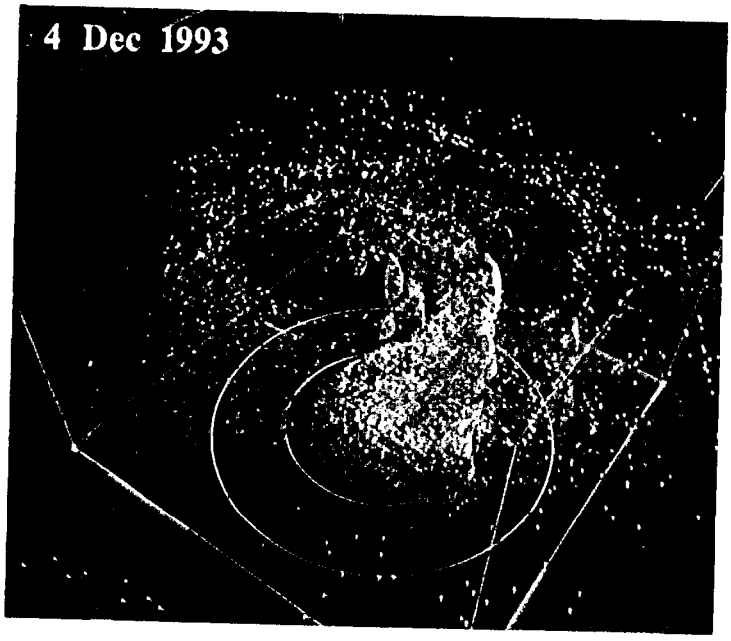
4 Dec 1993


7 Dec 1993

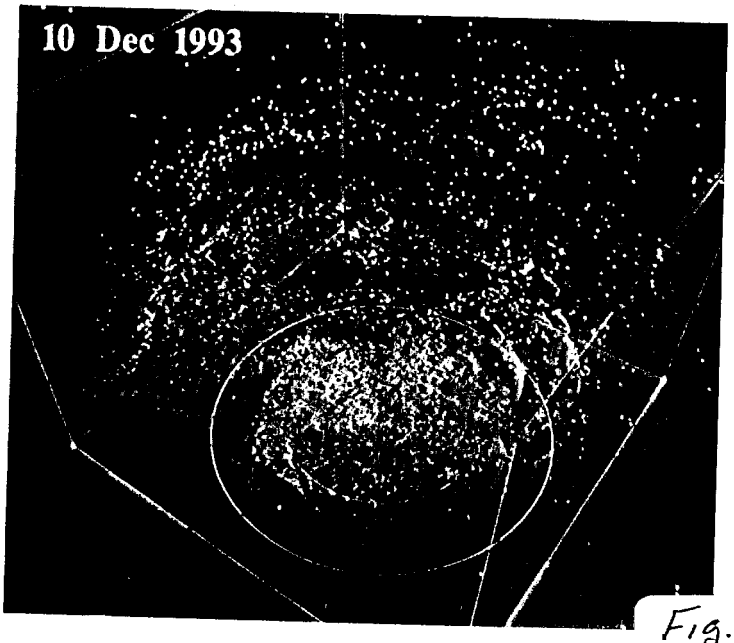
10 Dec 1993

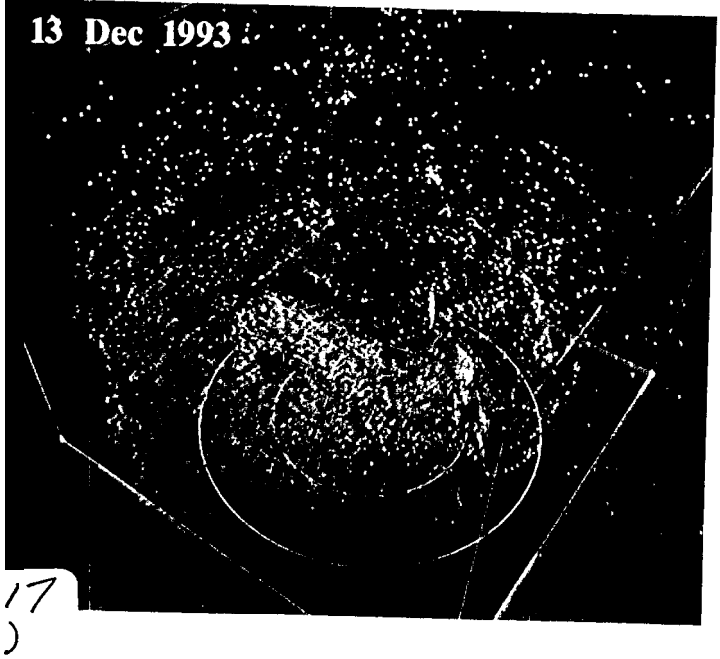
13 Dec 1993

Fig. 17
(3)

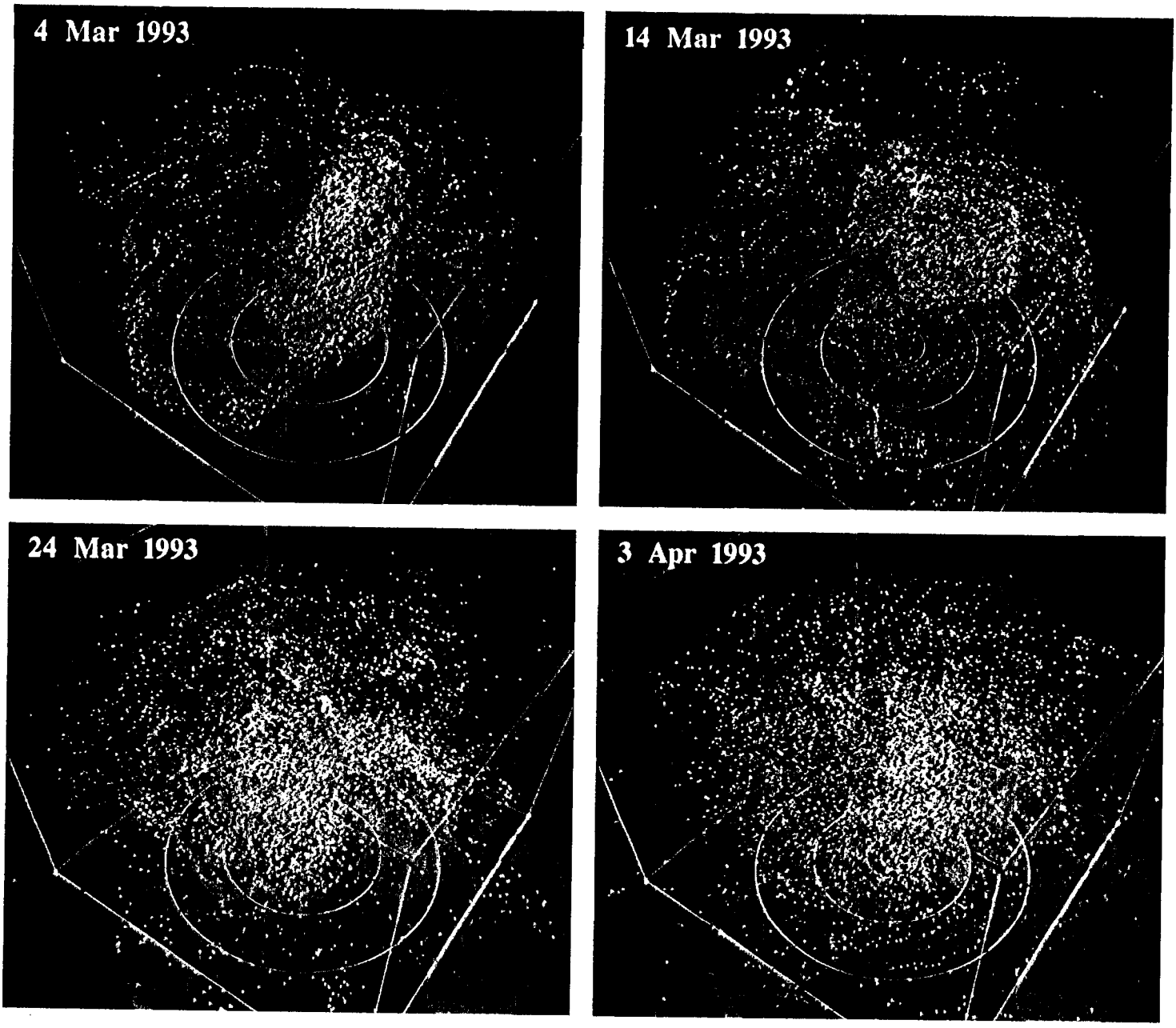

Fig. 18

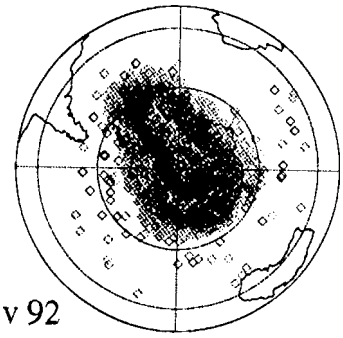

13N0v 92

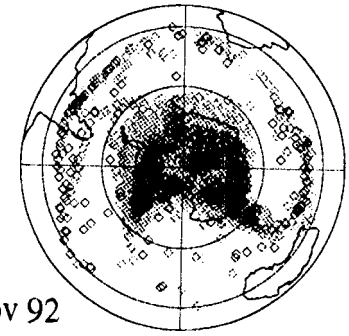

24 Nov 92

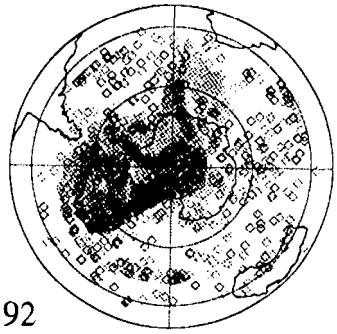

5 Dec 92

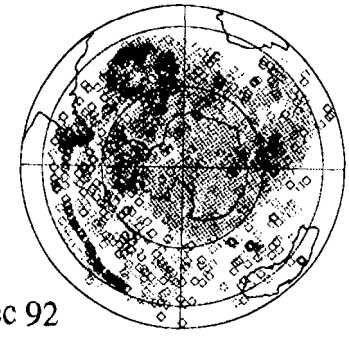

16 Dec 92

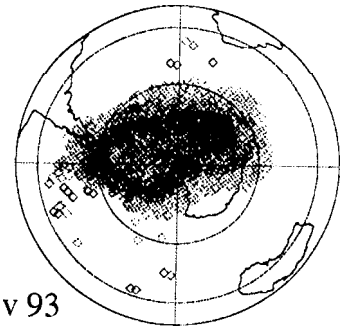

12N0v 93

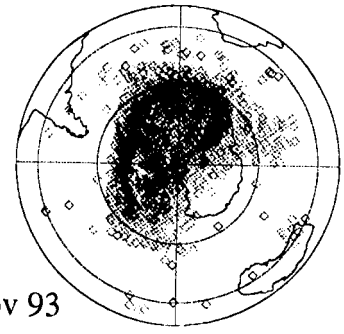

23 Nov 93

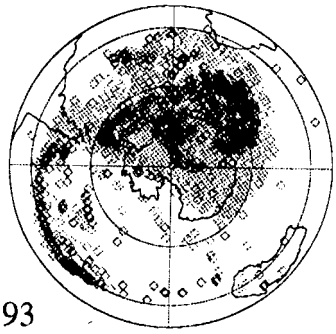

4 Dec 93

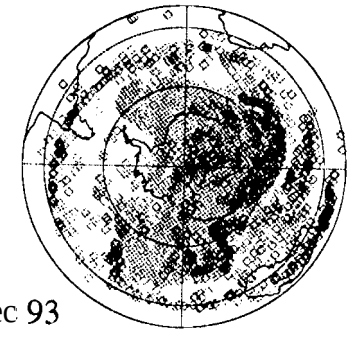

15 Dec 93

Fig. 19

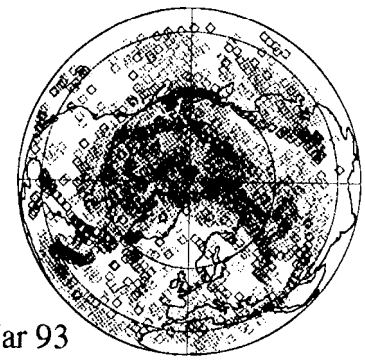

17 Mar 93

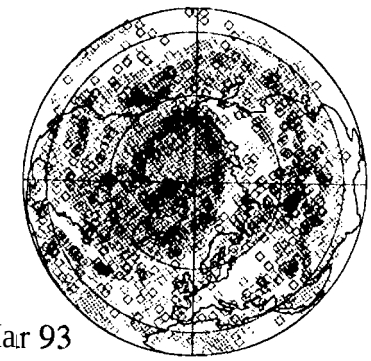

24 Mar 93

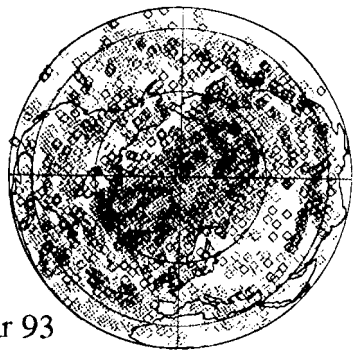

31 Mar 93

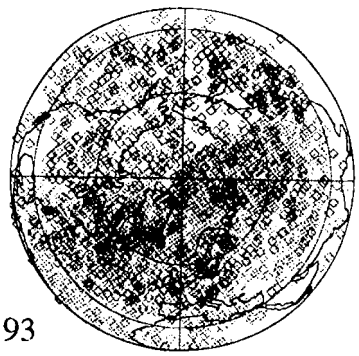

7 Apr 93

Fig. 19 cont.